



RESEARCH ARTICLE

10.1002/2017GC006798

Production, consumption, and migration of methane in accretionary prism of southwestern Taiwan

Key Points:

- We apply a systematic approach to quantify the rates of methane sources and sinks in different compartments in Taiwan accretionary prism
- CH₄ production and consumption rates at shallow depth were nearly offset by each other, leaving total effluxes less than production at depth
- The potential flux imbalance could be likely accounted for by the sequestration of methane into hydrate forms and the clay absorption

Supporting Information:

- Supporting Information S1
- Data Set S1
- Data Set S2
- Data Set S3

Correspondence to:

N.-C. Chen,
d00224005@ntu.edu.tw



Citation:

Chen, N.-C., et al. (2017), Production, consumption, and migration of methane in accretionary prism of southwestern Taiwan, *Geochem. Geophys. Geosyst.*, 18, doi:10.1002/2017GC006798.

Received 3 JAN 2017

Accepted 27 JUN 2017

Accepted article online 15 JUL 2017

Nai-Chen Chen¹ , Tsanyao Frank Yang¹, Wei-Li Hong^{1,2}, Hsuan-Wen Chen¹, Hsiao-Chi Chen¹, Ching-Yi Hu¹, Yu-Chun Huang¹, Saulwood Lin³, Li-Hung Lin¹, Chih-Chieh Su³, Wei-Zhi Liao³, Chih-Hsien Sun⁴, Pei-Ling Wang³, Tao Yang^{5,6}, Shao-Yong Jiang^{5,6}, Char-Shine Liu³ , Yunshuen Wang⁷, and San-Hsiung Chung⁷

¹Department of Geosciences, National Taiwan University, Taipei, Taiwan, ²Centre for Arctic Gas Hydrate, Environment and Climate, Department of Geology, UiT The Arctic University of Norway, Tromsø, Norway, ³Institute of Oceanography, National Taiwan University, Taipei, Taiwan, ⁴Exploration and Production Research Institute, CPC Corporation, Miaoli, Taiwan, ⁵State Key Laboratory for Mineral Deposits Research, Department of Earth Sciences, Nanjing University, Nanjing, China, ⁶Center of Marine Geochemistry Research, Department of Earth Sciences, Nanjing University, Nanjing, China, ⁷Central Geological Survey, MOEA, Taipei, Taiwan

Abstract To systematically quantify the production, consumption, and migration of methane, 210 sediment cores were collected from offshore southwestern Taiwan and analyzed for their gas and aqueous geochemistry. These data, combined with published results, were used to calculate the diffusive methane fluxes across different geochemical transitions and to develop scenarios of mass balance and constrain deep microbial and thermogenic methane production rates within the accretionary prism. The results showed that methane diffusive fluxes ranged from 2.71×10^{-3} to 2.78×10^{-1} and from -1.88×10^{-1} to $3.97 \text{ mmol m}^{-2} \text{ d}^{-1}$ at the sulfate-methane-transition-zone (SMTZ) and sediment-seawater interfaces, respectively. High methane fluxes tend to be associated with structural features, suggesting a strong structural control on the methane transport. A significant portion of ascending methane (>50%) is consumed by anaerobic oxidation of methane at the SMTZ at most sites, indicating effective biological filtration. Gas compositions and isotopes revealed a transition from the predominance of microbial methane in the passive margin to thermogenic methane at the upper slope of the active margin and onshore mud volcanoes. Methane production and consumption at shallow depths were nearly offset with a small fraction of residual methane discharged into seawater. The flux imbalance arose primarily due to the larger production of methane through deep microbial and thermogenic processes at a magnitude of $1512\text{--}43,096 \text{ Tg Myr}^{-1}$ and could be likely accounted for by the sequestration of methane into hydrate forms, and clay absorption.

1. Introduction

Atmospheric methane is ~ 23 times more effective in heat absorption than carbon dioxide on the basis of 100 year residence time [Forster *et al.*, 2007]. Even with ~ 200 times less concentration than carbon dioxide in the atmosphere, methane contributes 20–25% of the overall greenhouse effect [Lelieveld *et al.*, 1998]. Scenario modeling and geological records both have shown that its impact on climatic fluctuations over various timescales could have been substantial [Dickens *et al.*, 1995; Kennett *et al.*, 2000].

Marine sediments along continental margins have been estimated to store a total of $4.55 \times 10^5 \text{ Tg}$ of methane carbon, representing the largest methane reservoir on the Earth [Wallmann *et al.*, 2012]. Over the past few decades, great efforts have been dedicated to understanding the processes of methane cycling and to deconvolving the quantities of methane released from seafloor or seawater worldwide [Milkov, 2004; Wallmann *et al.*, 2012]. Of various tectonic settings, sediments eroded from high-relief mountainous area in tectonically active margins are rapidly deposited and accumulated at kilometer thickness, providing organic matter that is readily exploited for methane formation through thermal maturation and/or microbial degradation. Methane produced from either mechanism could be trapped as gas hydrate or in gas form within sediments in the subsurface [Katz *et al.*, 2002; Milkov *et al.*, 2005]. The substantial amount of carbon sequestered in active margins could become unstable and be transformed into the mobile phase caused by environmental fluctuations, such as temperature, sea level, and slope

stability, prior to ascending into the overlying seawater or even being discharged into the atmosphere [Judd and Hovland, 2007].

The ultimate release of methane from marine sediments is, however, controlled by multiple mechanisms and processes, such as thermal maturation of organic matter, microbial methanogenesis at depth, fluid channeling and sealing, hydrate sequestration, and biological filtration near the seafloor [Reeburgh, 2007; Hong *et al.*, 2017]. Although intensive methane cycling occurs along continental margins [Pohlman *et al.*, 2009; Archer and Buffett, 2012], very few studies have provided a quantitative framework to constrain the production, consumption, and migration of methane simultaneously at a regional scale in tectonically active environments. In particular, the overall methane inventory and leakage from different tectonic regimes could be greatly influenced by the supply, burial, and degradation of organic particulates. The lack of such knowledge limits a better assessment of the contribution of marine sediments to global methane emission.

In this paper, a systematic and comprehensive approach was adopted to quantify the rates for the methane sources and sinks from different compartments and to address the methane origin within the Taiwan accretionary prism. First, the diffusive fluxes of methane across the sulfate-methane-transition zone (SMTZ) and sediment-water interface were estimated by using 384 porewater profiles, 210 of which were newly reported here. The correlation between the fluxes and distribution of geological structure was discussed. Combined with the methane fluxes previously reported for terrestrial mud volcanoes [Yang *et al.*, 2004; Chao *et al.*, 2010; Hong *et al.*, 2013a], an estimate of the regional flux entering the seawater column and atmosphere was provided. The diffusion-based rates of anaerobic oxidation of methane (AOM) were also evaluated with the results independently obtained from the box model which considers the mass balance of solute concentrations and carbon isotopic compositions [Hong *et al.*, 2013b]. Second, the percentages of microbial to thermogenic methane production at great depth (>1 km) were constrained using published isotopic compositions of hydrocarbons from field samples and incubation experiments [Sun *et al.*, 2008; Ling *et al.*, 2012]. The potential rates of methane production by thermal maturation were assessed with the knowledge of sediment volume and properties, together with the rate and geometry of plate convergence for the accretionary prism. Finally, the hydrocarbon abundance ratios combined with their isotopic compositions from the cored bottom sediments were used to constrain the origins of hydrocarbon gases. Overall, we present a quantitative framework to assess the methane inventory within the Taiwan accretionary prism, and the possible source and sink mechanisms that control the methane leakages into surface environments. This study represents part of the outcomes for the decadal efforts in systematically exploring the distribution of methane seeps and hydrates as well as their environmental impacts off southwestern Taiwan.

2. Study Area and Geological Setting

Offshore southwestern Taiwan is a west advancing accretionary prism formed during the subduction of the Eurasian plate beneath the Philippine Sea plate starting about 18 Myr. The accretionary prism has obliquely impinged on the northern South China Sea margin through the collision between the Luzon Arc and Eurasian plate since 5 Myr [Teng, 1996; Lin *et al.*, 2008]. The uplift associated with the plate convergence generates extremely high rates of weathering and erosion onshore and drives rapid accumulation of organic matter in the abyssal plain of the northern South China Sea through numerous river systems [Dadson *et al.*, 2003; Hsu *et al.*, 2014]. With such a plate geometry, a transect from onshore to offshore southwestern Taiwan could be translated into a transition from active to passive continental margins. At the active margin, tectonic compression of the accreted terranes from the east generates a series of folds and thrusts propagating westward [Lin *et al.*, 2008]. The active margin consists two structural domains divided by the out-of-sequence thrust (OOST; Figure 1), namely, the lower slope and upper slope [Reed *et al.*, 1992]. At the upper slope, offshore mud diapiric structures and mud volcanoes are commonly observed [Chiang *et al.*, 2004]. These geological features could be further traced into their terrestrial counterparts that are aligned with the identified fault systems [Lin *et al.*, 2008]. In contrast, the lower slope consists of a series of anticlinal ridges related to active thrusting and folding [Lin *et al.*, 2008].

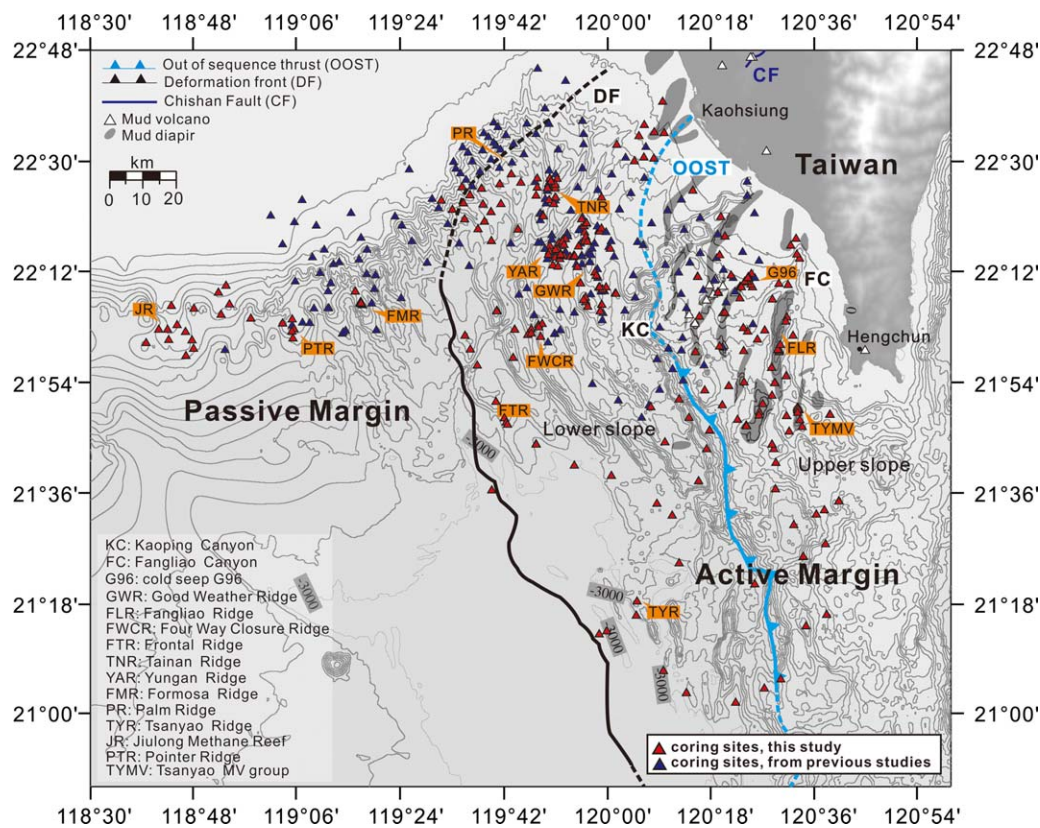


Figure 1. Map of coring sites offshore southwestern Taiwan (red triangles; $n = 210$). The locations of totally 384 sites were shown with 174 of them being previously reported (blue triangles) [Chuang *et al.*, 2006, 2010, 2013; Ye *et al.*, 2016]. The black line shows the deformation front (DF) and the blue line near the shelf edge denotes out of sequence thrust (OOST). The tectonic structures are modified from Lin *et al.* [2013].

3. Materials and Methods

3.1. Sediment and Core Top Seawater Samples

Sediment and core top seawater samples at 210 sites were retrieved during cruises of the R/V Ocean Researcher I (OR1; legs 804, 828, 834, 835, 860, 902, 934, 961, 978, 1029, 1044, 1070, 1107, and 1118), R/V Ocean Researcher III (OR3; legs 1323, 1368, 1384, and 1405), and R/V Ocean Researcher V (OR5; legs 1309–2 and 1311) using piston and gravity corers, and during R/V Marion Dufresne leg MD147 and MD178–10 using the Giant Piston Corer (GPC) and Calypso Square Corer (CASQ). Most sampling sites are located at (1) cold seep G96, Fangliao ridge (FLR), and Tsanyao mud volcano groups (TYMV) above mud diapirs; (2) Frontal ridge (FTR), Four way closure ridge (FWCR), Palm ridge (PR), Tainan ridge (TNR), and Tsanyao ridge (TYR) identified as anticlinal ridges; (3) Good weather ridge (GWR) and Yungan ridge (YAR) identified as monoclinal ridges; and (4) Formosa ridge (FMR) in the passive margin [Lin *et al.*, 2013]. Detailed sampling sites and core lengths are shown in Figure 1 and supporting information Table S1, respectively.

3.2. Sampling and Analytical Methods

Sediments (10 mL; 15 mL was used during MD178-10 cruise) and core top seawater for gas analyses were collected and transferred into serum bottles with saturated NaCl as a preservative. The serum bottles were sealed with butyl rubber stoppers, crimped with aluminum rings, and stored upside down at room temperature or 4°C. Pore water for aqueous geochemistry was obtained through centrifugation and subsequent filtration through a 0.22 μm pore-sized nylon membrane syringe filter. The filtrates were split into three fractions for anion, cation, and dissolved inorganic carbon (DIC) analyses. For cation analysis, concentrated nitric acid (70%) was added at a volume ratio of 1:45 for the preservation of redox sensitive metals. The DIC samples were collected in a 5 mL polypropylene vial without gas bubbles and stored at 4°C.

The concentrations of hydrocarbon gases were determined using gas chromatography (GC). Two approaches were used: (1) Samples obtained from MD147, OR1- 804, 828, 834, and 835 were analyzed using a GC equipped with a MS-13X (molecular sieve) column and a Hayesep D column in line with two thermal conductivity and one flame ionization detectors with H₂ and Ar as carrier gases (injection temperature 30°C, held isothermal for 2 min, ramped to 250°C at 120°C min⁻¹); (2) samples from other cruises were introduced into a GC equipped with a 4 m long Hayesep D column in line with a helium ionization detector. The temperature scheme for gas separation proceeded as the initial injection at 50°C, being held for 9 min, and ramped to 200°C at a rate of 90°C min⁻¹. Analytical precision is typically better than 5%.

Major ion concentrations (sulfate, calcium, and magnesium) were determined using an ion chromatography (882 Compact IC Plus) with a detection limit of 0.1 ppm in weight. Total alkalinity was determined by titrating the sample with 0.02 N HCl while bubbling nitrogen through the sample [Wallmann *et al.*, 2006a]. The concentrations and carbon isotopic compositions of DIC were measured using an OI Analytical total organic carbon (TOC) analyzer combined with a Picarro G1101-*i* cavity ring down spectrometer (CRDS) isotopic analyzer. A total of 10–15 mL of water sample was treated with 5% H₃PO₄ in a glass vial at 25°C on line. The CO₂ produced was stripped with N₂ and introduced into the detectors. The carbon isotopic compositions of methane were measured using a Methane Carbon Isotope Analyzer (MCIA) equipped with a tunable diode laser absorption spectrometry or an isotope ratio mass spectrometry (IRMS) in line with a GC and a combustion oven. The hydrogen isotopic compositions of methane were determined using an IRMS in line with a GC and a pyrolysis oven. The obtained isotopic compositions were expressed as the δ notation referenced to standards [$\delta = (R_{\text{sample}}/R_{\text{std}} - 1) \times 1000\text{‰}$, where R is the ratio of heavy to light isotopes]. The standards for carbon and hydrogen isotopes are the Pee Dee Belemnite (PDB) and Vienna Standard Modern Ocean Water (VSMOW), respectively. The precisions are $\pm 0.5\text{‰}$ – 1‰ for CRDS measurements, $\pm 0.5\text{‰}$ – 1‰ for MCIA measurements, and $\pm 0.5\text{‰}$ for $\delta^{13}\text{C}$ -methane and $\pm 3\text{‰}$ for $\delta^2\text{H}$ of methane by the IRMS.

3.3. Calculations of Fluxes Across Different Interfaces

The diffusive fluxes of methane across the SMTZ were calculated using the Fick's first law [Berner, 1980],

$$F = -\varphi \cdot D_s \cdot \frac{\partial C}{\partial x}, \quad (1)$$

where F is the flux, φ is the porosity converted from water content assuming a sediment density of 2.7 g cm⁻³ [Chen, 1981], D_s is the bulk sediment diffusion coefficient corrected for tortuosity, C is the methane concentration, and x is the depth. D_s was calculated using equation (2).

$$D_s = D_w / (1 - \ln(\varphi^2)), \quad (2)$$

where D_w is the diffusion coefficient in seawater at in situ temperatures [Jähne *et al.*, 1987; Boudreau, 1997]. Because the measured methane quantity represents the residual fraction postdegassing during core recovery, the calculated diffusive flux is a conservative estimate. Raw data of methane and sulfate concentration are listed in supporting information Table S2.

Fluid advection is assumed negligible. The assumption was based on the profiles of chloride which is inert to biological and most abiotic reactions, thereby serving the best tracer for fluid migration. Deeply sourced fluids are commonly characterized with low salinity derived from either hydrate dissociation or clay dehydration [Kastner *et al.*, 1991]. The contrast chloride concentrations between deeply sourced fluid and seawater render chloride a sensitive tracer to investigate whether advection is significant and affects the shallow-ranging geochemical characteristics. Of 101 sites (including sites described in previous studies [Chuang *et al.*, 2013; Lin *et al.*, 2014; Ye *et al.*, 2016]) with chloride data available (supporting information Table S2), most sites (94 sites) were characterized with no or insignificant changes in chloride concentration, suggesting small contribution of advection in these shallow sediments. Only seven sites proximal to mud volcanoes, mud diapirism or structural features are characterized by downward decreasing chloride concentrations. The chloride profiles from six of them (OR1-1070-C11, OR1-1070-C9, MD178-3292, MD178-3280, OR1-902A-9, and OR1-1107-MV12-1) showed a linear decreasing trend, whereas the other one (OR1-1107-MV12-A) exhibited a concave downward shape. The linear decreasing of chloride content indicating the dominance of diffusion, whereas the concave-downward profile suggests the combinative effect of diffusion and advection only on this site. To constrain the advection rate, the fluid transport

equation (combining diffusion and advection) was used to fit the observed chloride variation. Our calculation yielded an advection rate of $\sim 0.4 \text{ cm yr}^{-1}$. Such an advection rate could be translated into an advective methane flux of $1.55 \times 10^{-1} \text{ mol m}^{-2} \text{ yr}^{-1}$ at the SMTZ (using a porosity of 0.35 and a methane concentration of 0.11 mM). The diffusive flux across the SMTZ was calculated to be $3.80 \times 10^1 \text{ mol m}^{-2} \text{ yr}^{-1}$, a magnitude approximately 240 times greater than the advective flux. Therefore, the advective flux could be considered negligible even in the region with relatively high fluid flow. The modeling calculation also demonstrates that unless the sampling was conducted right at the structural features, the majority of sampling area is governed by diffusive transport of methane.

Methane concentration gradients were calculated from the depth intervals where the concentrations linearly increased. Linear regression was then applied to the target depth of interest. For methane fluxes across the SMTZ, at least three data points across the sulfate minimum to methane minimum were used for the analyses. Methane concentration data from 64 sites (with 20 sites reported by from *Chuang et al.* [2006, 2010, 2013], *Lin et al.* [2014], and *Ye et al.* [2016]) were calculated. The fluxes at 11 sites obtained from *Chuang et al.* [2010] were included for comparison. The obtained diffusive fluxes across the SMTZ were further categorized into two groups using a probability plot from which the flux corresponding to the drastic change of flux to frequency ratio was selected as the threshold value for categorization [*Sinclair, 1974*]: hot sites with fluxes more than $10^{-1} \text{ mmol m}^{-2} \text{ d}^{-1}$ and normal sites with fluxes lower than $10^{-1} \text{ mmol m}^{-2} \text{ d}^{-1}$. The ranges of flux were multiplied with the areas to obtain the total area-based methane consumption rates, considering that this geochemical transition resulted from the AOM process alone. Using the distribution of sites, the areas of the passive margin and active margin for normal sites were calculated to be 3400 and 11,777 km^2 , respectively (supporting information Figure S1). The areas of all hot sites were estimated to range from 0.11 to 40.7 km^2 . To simplify the calculation and avoid the contributions from extreme values, a minimum area of 0.11 km^2 was used to represent all hot sites. We estimated the area occupied by hot sites from the distribution of methane flux across the sediment-water interface as the coverage of this sampling is large enough for representative estimation. The resulting area of hot sites on the passive and active margins are 0.33 ($n = 2$) and 2.86 ($n = 26$) km^2 , respectively.

The diffusive boundary layer (DBL) is defined as the interface between seawater and sediment. Methane effluxes across the DBL were calculated using the following equation [*Jørgensen and Des Marais, 1990*]:

$$F_{DBL} = D_w \cdot \frac{C_0 - C_w}{Z_{diff}}, \quad (3)$$

where F_{DBL} is the flux across the sediment-seawater interface (i.e., efflux), C_0 is the methane concentration immediately below the DBL in the surficial sediments, C_w is the concentration in the bottom water, and Z_{diff} is the thickness of DBL and is assumed to be 1.0 mm [*Boudreau and Guinasso, 1982*]. Because C_0 is an unknown value, the mass balance relationship between the methane efflux across the DBL and methane flux at the top sediments was adopted to derive C_0 and hence the efflux using the following equation [*Dale et al., 2008b*]:

$$D_w \cdot \frac{C_0 - C_w}{Z_{diff}} = \varphi_0 \cdot \left(D_s \cdot \frac{C_1 - C_0}{\Delta x} - v \cdot C_0 \right), \quad (4)$$

where φ_0 is the sediment porosity at the seabed, C_1 is the methane concentration at the grid node immediately below C_0 , Δx is the distance between depths of C_0 and C_1 , and v is the advective flow rate. The methane concentration at the shallowest depth of the core was used as C_1 , whereas v was assumed to be negligible. For sites without methane concentrations of bottom water, C_w for sites nearby was used. Methane concentration data from 370 sites (with 171 sites collected from *Chuang et al.* [2006, 2010, 2013]) were calculated.

The calculated effluxes at specific sites were further extrapolated to derive the area-based discharge of methane into seawater. Following a similar approach described above, the obtained diffusive effluxes were further categorized into normal and hot sites using an arbitrary threshold value of $10^{-2} \text{ mmol m}^{-2} \text{ d}^{-1}$. The ranges of flux were multiplied by the areas to obtain the total quantity of methane discharged per unit time. The area sizes for individual categories were the same as those described previously. These marine effluxes were compared with the published methane emission from terrestrial mud volcanoes [*Yang et al., 2004; Chao et al., 2010; Hong et al., 2013a*] and from submarine environments elsewhere.

3.4. Methane Production and Consumption Constrained by the Box Model

The methane production and consumption rates (or fluxes) at the SMTZ were calculated to evaluate the diffusion-based AOM rates independently using the solute and isotopic data available at these depth ranges. The box model [Hong *et al.*, 2013b] which considers the mass balance between five reactions, organotrophic sulfate reduction (OSR), AOM, carbonate precipitation (CP), methanogenesis (ME), and CO₂ reduction (CR), were employed. CR represents the reversible pathway that is accompanied internally with AOM [Yoshinaga *et al.*, 2014], whereas methanogenesis (ME) produces methane from the degradation of organic matter. Although the product is the same, these two reactions are intrinsically different and involve different populations. Fluxes from deep sources are used to satisfy the mass balance at the SMTZ (supporting information Table S3). Methane flux was derived by subtracting the total sulfate reduction rate from the sulfate consumption with organic matter, assuming that methane-fueled AOM is responsible for the rest of the sulfate reduction. The gradients of SO₄²⁻, Ca²⁺, Mg²⁺, and DIC were used to derive the fluxes or rates for individual reactions. Carbon isotopes were used as an additional constraint. The carbon isotopic fractionation factors related to AOM and CR were assumed to be 1.004 and 1.06, respectively [Whiticar, 1999]. While most organic matter can be degraded in shallow sediments through OSR, the rest is buried into the methanogenic zone for methane production. The partition factor of organic degradation via OSR was assumed to be 0.8 based on the modeling results from Chuang *et al.* [2013]. Because of the data availability, 11 sites (supporting information Figure S2 and Table S3) were chosen for model calculations, and all the geochemical characteristics were assumed to reach a steady state. Since the site numbers were small, no categorization for hot versus normal sites was performed. The calculated AOM rates were compared to those obtained from the concentration gradients to validate the diffusive fluxes. The calculated methane production and AOM rates were also used to assess the methane mass balance at shallow depth.

3.5. Fractions of Microbial Methane Production at Great Depth

The absolute quantity of deep microbial methane production (>1 km) was obtained by combining the fraction of pure microbial to thermogenic methane with the rates of thermogenic methane production deduced from subduction geometry and parameters (see section 3.6). The fraction of deep microbial methane production was first estimated using published isotopic compositions of hydrocarbons collected from the bubbling pools of terrestrial mud volcanoes [Sun *et al.*, 2008, 2010]. The generalization of terrestrial for marine environments stems from the fact that sediments in both compartments share genetic relationships. As plate convergence has been driven by the accretion of the Luzon arc for at least 9.7 Myr [Huang *et al.*, 2006], all sediments previously deposited offshore southwestern Taiwan would be subject to a similar path of burial and tectonic displacement or deformation, regardless of deposition time. Therefore, sediments currently located at great depth in both terrestrial and marine compartments were assumed to retain similar reactivity for microbial methane formation. While sediment retrieval directly from great depth in marine environments is not yet available, fluids and sediments from the bubbling pools of terrestrial mud volcanoes are perhaps the best alternative materials to characterize the source of deep fluid, considering that rapid fluid transport along fractures prevents the geochemical characteristics of pool fluids and sediments from being altered or modified [Ling *et al.*, 2012; Wang *et al.*, 2014].

The following equation was used to obtain the fractions of microbial and thermogenic methane from great depths.

$$\delta^{13}\text{C}_{\text{measured}} = \delta^{13}\text{C}_m \times f_{\text{mgd}} + \delta^{13}\text{C}_t \times (1 - f_{\text{mgd}}), \quad (5)$$

where $\delta^{13}\text{C}_{\text{measured}}$ is the measured $\delta^{13}\text{C}$ value of methane, $\delta^{13}\text{C}_m$ is the $\delta^{13}\text{C}$ value of microbial end-component, $\delta^{13}\text{C}_t$ is the $\delta^{13}\text{C}$ value of thermogenic methane, and f_{mgd} represents the fraction of microbial methanogenesis at great depth.

To obtain the isotopic composition of pure thermogenic methane ($\delta^{13}\text{C}_t$ in equation (5)), the natural gas plot was adopted [Chung *et al.*, 1988; Milkov and Dzou, 2007]. This approach lies in the rationale that the $\delta^{13}\text{C}$ value and the reciprocal of carbon number of hydrocarbon ($1/n$) would follow a linear relationship for hydrocarbons produced purely by thermogenesis. The slope and intercept at $1/n$ of 0 could be translated to the maturity and initial composition of a hydrocarbon source, respectively. Published $\delta^{13}\text{C}$ values of hydrocarbons (C₁-nC₅) retrieved from gas seeps and mud volcanoes in southwestern Taiwan [Sun *et al.*, 2008, 2010] were applied to the natural gas plot. A threshold of R² value at 0.9 obtained from linear regression

Table 1. Summary of $\delta^{13}\text{C}$ Values of Hydrocarbons From Onshore Mud Volcanoes and Seeps, Projected $\delta^{13}\text{C}$ Values of Pure Thermogenic Methane, and Potential Contribution of Microbial Methanogenesis

Sample Name	Measured $\delta^{13}\text{C}$ (‰) ^a					Projected $\delta^{13}\text{C}$ (‰) From Natural Gas Plot			f_{mgd}		
	C ₁	C ₂	C ₃	nC ₄	nC ₅	Thermo C ₁ ($\delta^{13}\text{C}_t$)	Hydrocarbon Source	Δ ($\delta^{13}\text{C}_m - \delta^{13}\text{C}_p$) ^b	Acetoclastic Fraction ^c	CO ₂ Reduction Fraction ^d	CO ₂ Reduction Fraction ^e
KTL-06	-32.9	-23.5	-23.9	-24.0	-23.7	-23.8	-23.8	-9.1	0.49	0.24	0.16
CLB-B12	-26.5	-25.3	-24.5	-24.0		-26.6	-23.4	0.1	0.00	0.08	0.05
CLB-SW06	-33.0	-24.1	-24.8	-24.8		-24.6	-24.6	-8.4	0.47	0.22	0.15
YNH-12	-31.3	-27.7	-24.3	-24.7	-24.7	-31.4	-22.5	0.1	0.00	0.22	0.15
SYNH-10	-31.6	-25.9	-25.2	-25.2	-25.6	-31.1	-23.0	-0.5	0.04	0.22	0.14
WSD-04	-30.3	-26.3	-22.3	-23.5		-30.4	-20.3	0.1	0.00	0.24	0.16
LYS-02a	-29.9	-24.3	-26.7	-25.6		-25.5	-25.5	-4.4	0.26	0.12	0.08
KSP-12	-51.0	-36.0	-30.2	-27.6		-51.1	-20.0	0.1	0.01	0.73	0.50
95G908	-33.2	-25.3	-23.5	-23.6	-23.5	-32.7	-20.0	-0.5	0.05	0.31	0.21
95G925	-33.4	-19.2	-15.6	-18.3		-32.5	-9.7	-0.9	0.09	0.45	0.33
95G926	-32.7	-24.8	-26.3	-26.2	-25.9	-25.8	-25.8	-6.9	0.41	0.19	0.12
95G907	-27.9	-24.2	-23.9	-24.3	-24.1	-24.1	-24.1	-3.8	0.21	0.10	0.07
95G924	-29.6	-23.2	-22.7	-24.5		-23.5	-23.5	-6.1	0.32	0.16	0.10
95G913	-31.3	-26.6	-24.6	-24.7	-24.4	-31.2	-22.2	-0.1	0.01	0.23	0.15
95G927	-39.0	-26.8	-24.6	-24.1	-23.6	-38.3	-19.7	-0.7	0.17	0.45	0.31

^aTerrestrial mud volcano data source from Sun et al. [2008, 2010].

^b $\Delta(\delta^{13}\text{C}_m - \delta^{13}\text{C}_p)$ represents the difference of $\delta^{13}\text{C}$ values between measured methane and projected pure thermogenic methane.

^cPotential contribution of acetoclastic methanogenesis to the total methane was calculated on the basis of equation (5) and a fractionation factor of 1.020 obtained from incubation experiments [Ling et al., 2012].

^dPotential contribution of CO₂ reduction fraction to the total methane was calculated on the basis of equation (5) and a fractionation factor of 1.040 [Ling et al., 2012; Whiticar, 1999].

^ePotential contribution of CO₂ reduction fraction to the total methane was calculated on the basis of equation (5) and a fractionation factor of 1.060 [Whiticar, 1999].

was arbitrarily chosen in order to determine whether the $\delta^{13}\text{C}$ values of C₁-nC₅ were linearly distributed (supporting information Figure S3a). For the covariance between $\delta^{13}\text{C}$ value and $1/n$ (R^2 values greater than 0.9), the equation generated from regression was used to calculate the $\delta^{13}\text{C}$ values of pure thermogenic methane and hydrocarbon source. For regression with R^2 values less than 0.9, the $\delta^{13}\text{C}$ values of C₂₊ generally clustered within $\pm 1\text{‰}$, and were, therefore, averaged and extrapolated to $1/n$ of 1 and 0 for the determination of $\delta^{13}\text{C}$ values of pure thermogenic methane and hydrocarbon source, respectively (supporting information Figure S3b). Since microbial oxidation and synthesis would leave the residual hydrocarbons (mostly C₁, C₃, and C₄) enriched in ¹³C and produce ¹³C-depleted methane [James and Burns, 1984], such an analysis allows for the identification of potential microbial processes that deviate $\delta^{13}\text{C}$ values of hydrocarbons from the predictive thermogenic trend. The projected $\delta^{13}\text{C}$ values of pure thermogenic methane ($\delta^{13}\text{C}_t$, Table 1) combined with the $\delta^{13}\text{C}$ values of pure microbial methane produced from the decomposition of organic matter (see next paragraph) were further used to estimate the microbial contribution to the overall methane inventory through equation (5).

Three scenarios were considered to constrain the $\delta^{13}\text{C}_m$ values in equation (5). In any scenarios, the isotopic fractionation between particulate organic matter and methanogenic precursor was assumed to be negligible. Therefore, the $\delta^{13}\text{C}$ value of pure microbial methane could be deduced by subtracting the $\delta^{13}\text{C}$ value of particulate organic matter with the isotopic fractionation associated with methanogenesis. The $\delta^{13}\text{C}$ values of the projected source composition or organic matter in offshore sediments [Hsu et al., 2014, and this study] clustered mostly between -25 and -20‰ . Therefore, a median value of -22.5‰ was chosen to represent the isotopic composition of organic matter subject to microbial degradation. The first scenario considered assumes that the predominant methanogenic pathway was through acetate fermentation with a carbon isotope fractionation of 20‰ . This assumption is based on the incubation results using mud volcano sediments in the region as inoculum and acetate as substrate [Ling et al., 2012]. The $\delta^{13}\text{C}_m$ value was calculated to be -42.5‰ ($-22.5 - 20\text{‰} = -42.5\text{‰}$). The second and third scenarios focused on methanogenesis through CO₂ reduction with carbon isotopic fractionations of 40 and 60‰ [Ling et al., 2012; Whiticar, 1999], respectively. For these two scenarios, the $\delta^{13}\text{C}_m$ values were calculated to be -62.5 and -82.5‰ , respectively. The obtained f_{mgd} (Table 1) was further transformed into the microbial-to-thermogenic ratio, and multiplied by the total thermogenic methane production (see the section 3.6) to derive the quantity of regional microbial contribution.

3.6. Thermogenic Methane Produced by Subduction and Accretion

The production rate of thermogenic methane within the accretionary prism was estimated based on the following equation proposed by Schmoker [1994],

$$R_{\text{thermo}} = R_{\text{acc-M}} \cdot m \cdot PP, \quad (6)$$

where R_{thermo} is the production rate of thermogenic methane, $R_{\text{acc-M}}$ is the sediment mass accumulated within the accretionary prism, m is the maturity of the sediments, and PP is the hydrocarbon potential of the sediments (i.e., the weight of hydrocarbon per unit weight of sediments). To determine the m value, the following two assumptions were made:

1. Seventy percent of sediments were assumed to subduct along with the plate, with the remaining 30% of sediments being accreted [von Huene and Scholl, 1991]. All the sediments being subducted were assumed to be totally matured once they reached the depth of the gas window. This assumption ignores the possibility that subducted organic matter could be completely oxidized to CO_2 or graphitized. The remaining 30% accreted sediments could be matured for hydrocarbon formation if the sediments are buried to a depth greater than 1.29 kmbsf considering an average geothermal gradient of 70°C km^{-1} [Chi and Reed, 2008] and 90°C for the gas window. Based on the seismic reflection signals near the current trench and deformation front, the thickness of presubducted sediments was calculated to be 1.24–4.49 km [Yeh and Hsu, 2004; Liao et al., 2016]. The contribution of thermogenic methane from such accreted sediments is small and insignificant. For example, the greatest thickness of pre-subducted sediments is 4.49 km. The thickness of accreted sediments would be less than 1.35 km ($4.49 \text{ km} \times 30\%$). The proportion of accreted sediments immediately subject to thermal maturation at subduction would be only 1.3% ($(1.35 - 1.29) \text{ km} / 4.49 \text{ km} \times 100\%$). The fraction will be even smaller for the presubducted sediments that is thinner than 4.49 km. Moreover, the thickness of pre-subducted sediments more than 4 km is only representing 11% of the trench in length. As the potential accreted sediments for thermal maturation is small and the exact accretion rate has not been constrained well, the thermogenic methane contributed from the accreted sediments was assumed to be negligible.
2. Given that 40% of the total hydrocarbons are in cyclic structures and resistant to thermal decomposition, all the other hydrocarbons were assumed to be eventually converted to methane under high temperatures and pressures [Hunt, 1996]. Therefore, m was calculated to be 42% ($70\% \times 0.6 = 42\%$). Based on the results from the four ODP sites (ODP leg184, Site 1144, 1145, 1146, and 1148; at the northern slope of the South China Sea [Wang et al., 2000]), the values of hydrocarbon potential (PP in equation (6)) were assumed to be 0.15–0.5 mg of hydrocarbon per kg sediments.

$R_{\text{acc-M}}$ in equation (6) was calculated by assuming a simplified geometry of the accretionary prism (Figure 2) and the density of bulk sediments (ρ_{bulk}) using the following equation:

$$R_{\text{acc-M}} = R_{\text{acc-V}} \cdot \rho_{\text{bulk}}, \quad (7)$$

where $R_{\text{acc-V}}$ is the rate of sediment volume accumulated, calculated by the following equation [von Huene and Scholl, 1991]:

$$R_{\text{acc-V}} = H_{\text{tr}} \cdot L_{\text{tr}} \cdot R_{\text{sd}}, \quad (8)$$

where H_{tr} is the thickness of the sediments in the trench, L_{tr} is the length of the trench, and R_{sd} is the subduction rate. Specifically, the thickness of sediments in the trench (H_{tr}) was assumed to be 1.24–4.49 km (described above). The length of trench (L_{tr}) was calculated to be 400 km (from 21°N to 24.5°N) based on the definition by Chi et al. [2003] and Huang et al. [2006]. Because the investigated area represents 71% of the whole trench in length (from 21°N to 23.5°N), the trench length used in the model calculation was assumed to be 284 km (Figure 2). The subduction rate (R_{sd}) was assumed to be 66–76 km Myr^{-1} [Suppe, 1981; Lundberg et al., 1997]. In order to convert the volume of sediments to its mass ($R_{\text{acc-M}}$), porosity and ρ_{bulk} values from ODP sites mentioned above were used [Wang et al., 2000]. The obtained quantity represents the volume of methane potentially formed through the subduction and accretion for the investigated trench length. All parameters used in the calculation are summarized in supporting information Table S4.

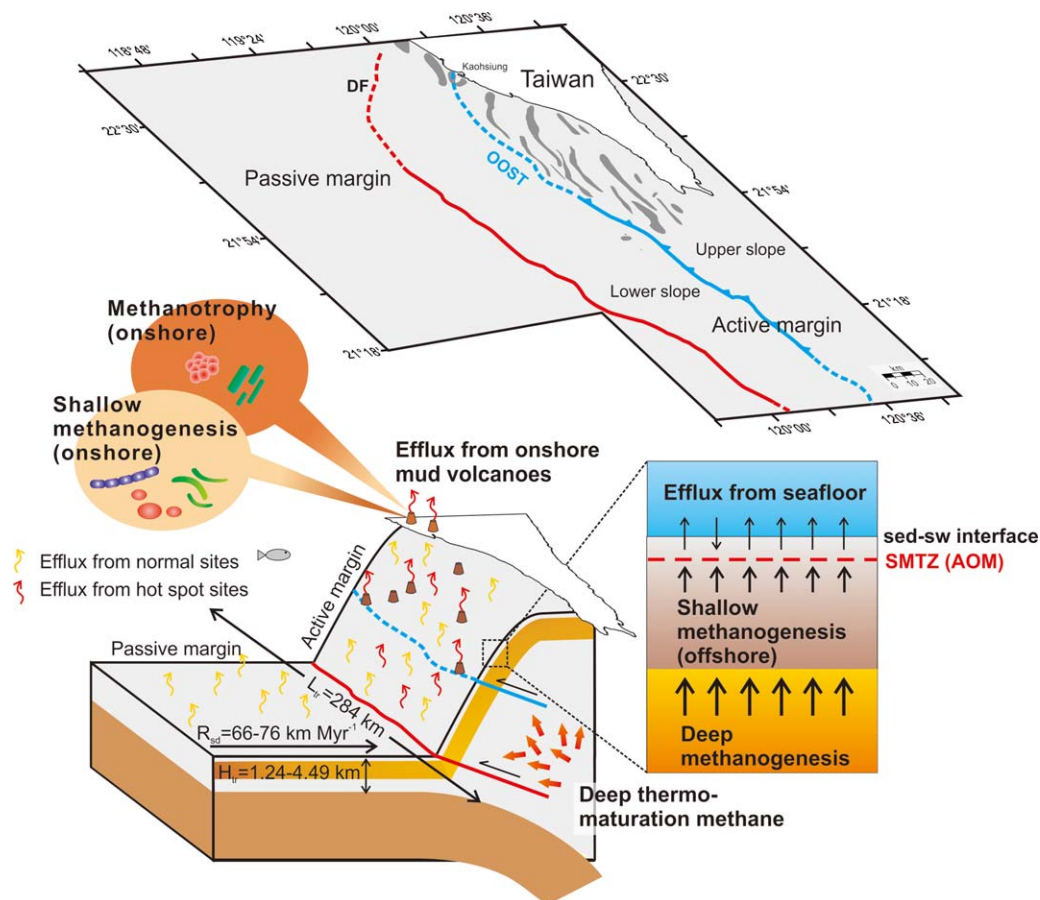


Figure 2. Conceptual framework of methane cycling and transport and from various tectonic compartments of the Taiwan accretionary prism. All processes considered for methane effluxes, sinks, and sources are shown. The red line shows the deformation front (DF) and the blue line near the shelf edge denotes out of sequence thrust (OOST) [Lin *et al.*, 2013].

4. Results

4.1. Methane Fluxes Across Geochemical Transitions at Shallow Depth

The calculations yielded diffusive methane fluxes ranging from 2.71×10^{-3} to 2.78×10^{-1} $\text{mmol m}^{-2} \text{d}^{-1}$ ($n = 64$, Figure 3) across the SMTZ, and from -1.88×10^{-1} to 3.97×10^0 $\text{mmol m}^{-2} \text{d}^{-1}$ at the sediment-seawater interface ($n = 370$; Figure 4; 29 sites had negative values; supporting information Table S1). For the SMTZ, fluxes at most sites were in the range between 10^{-2} and 10^{-1} $\text{mmol m}^{-2} \text{d}^{-1}$. Fluxes with higher values (more than 10^{-1} $\text{mmol m}^{-2} \text{d}^{-1}$) were observed predominantly at ridges and seep area, including sites at TNR ($0.32 \text{ mmol m}^{-2} \text{d}^{-1}$), FTR ($0.25 \text{ mmol m}^{-2} \text{d}^{-1}$), area between YAR and GWR ($0.23 \text{ mmol m}^{-2} \text{d}^{-1}$), and cold seep G96 ($0.11 \text{ mmol m}^{-2} \text{d}^{-1}$; Figure 3 and supporting information Figure S4). Combined 11 sites with previous results [Chuang *et al.*, 2010] and area coverage, the area-based methane consumptions mediated by AOM were from 188 to 5976 (mean = 2054) Mg yr^{-1} in the active margins. Since only one site of flux across SMTZ was obtained in the passive margin, no area-based flux was calculated. For the sediment-seawater interface, the effluxes at most sites were between 10^{-5} and 10^{-3} $\text{mmol m}^{-2} \text{d}^{-1}$. Most effluxes in active margin were around 10^{-4} $\text{mmol m}^{-2} \text{d}^{-1}$ and around 10^{-5} $\text{mmol m}^{-2} \text{d}^{-1}$ in the passive margin (Figure 4). Sites at cold seeps G96, TYMV, and FMR exhibited particular higher fluxes (more than 10^{-1} $\text{mmol m}^{-2} \text{d}^{-1}$). The few negative fluxes were excluded from further calculation of area-based effluxes, because the high methane concentrations of bottom seawater might result from the disturbance caused by the coring penetration. With the area coverage described above, the area-based methane effluxes were 0.04–47.0 (mean = 4.21) Mg yr^{-1} and 0.3–683 (mean = 52.0) Mg yr^{-1} in the passive and active margins, respectively.

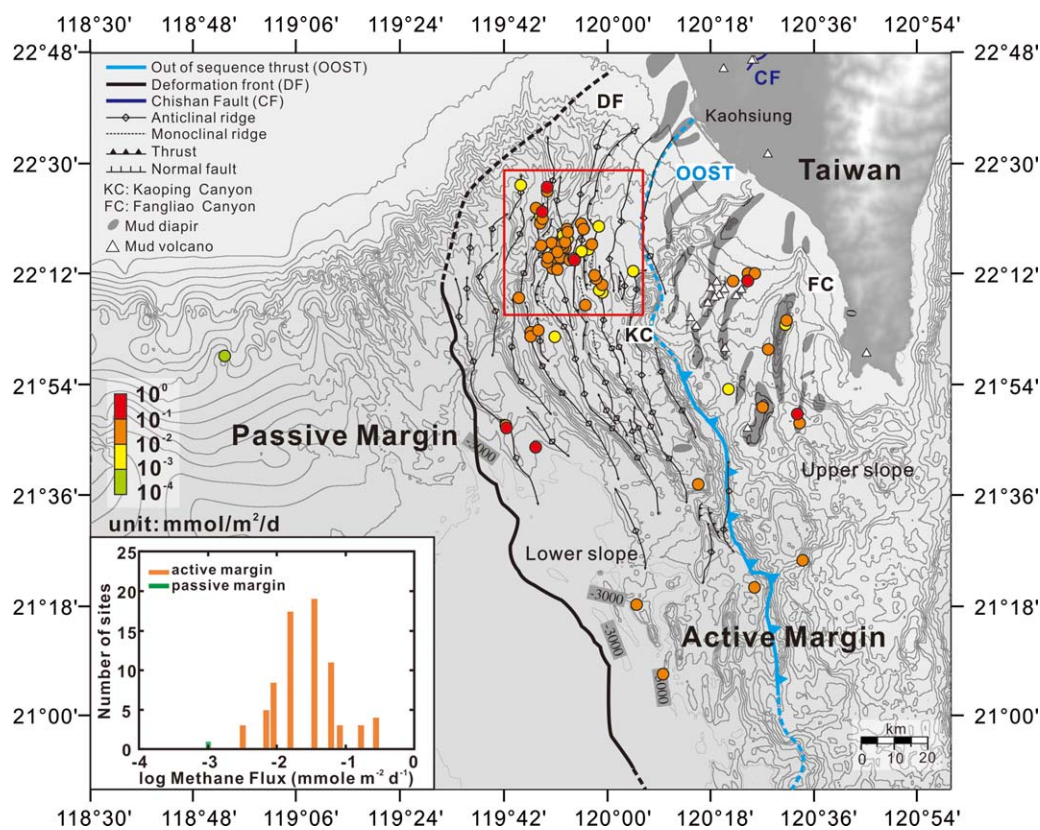


Figure 3. Methane fluxes across the SMTZ of the investigated area ($n = 75$). The red rectangle defines the region with intensive sampling, and enlarged as shown in supporting information Figure S4. The tectonic structures are modified from Lin et al. [2013]. Part of data used for calculation was adopted from Chuang et al. [2013] and Ye et al. [2016]. The fluxes obtained from Chuang et al. [2010] are included for comparison ($n = 11$).

4.2. Methane Production and Consumption at Shallow Depth

AOM, OSR, CP, CR, and ME rates derived from the box model for the SMTZ zone at 11 sites ranged from 0.08 to 2.42, 0.07 to 1.15, 0.15 to 1.92, 0.17 to 0.84, and 0.04 to $0.57 \times 10^{-1} \text{ mmol m}^{-2} \text{ d}^{-1}$, respectively (supporting information Table S3). AOM accounted for the majority of sulfate consumption at seven sites (AOM/OSR ratios exceeded 1.7; supporting information Table S3), whereas rates of AOM and OSR were nearly equivalent (the proportion of sulfate consumed by AOM ranged between 43 and 53%) at the other three sites. The AOM rates derived from the box model were comparable with diffusive fluxes for sites C17, EN1, C5, 3289, and 3280 (supporting information Table S3), but were greater than diffusive fluxes by a factor of 3.2–5.6 for the remaining sites. The overall methane production (ME+CR) was 0.3–1.7 times the consumption (AOM) rates.

4.3. Microbial and Thermogenic Methane Production at Great Depth

The natural gas plot (supporting information Figures S3 and S5) was applied to project the isotopic composition of the pure thermogenic methane. Of the 15 data sets, 6 sets (terrestrial mud volcanoes: CLB-SW06, KTL-06, LYS-02A, 95G926, 95G907, and 95G024) that did not meet the R^2 threshold (R^2 value < 0.9) obtained from the regression analysis exhibited almost invariant $\delta^{13}\text{C}$ values of C_{2+} compounds (Table 1). The extension of averaged $\delta^{13}\text{C}$ values of C_{2+} to $1/n$ of 1 predicted the $\delta^{13}\text{C}$ values ranging between -25.8 and -23.8‰ for methane produced purely by thermal maturation. The offsets between the predicted and measured $\delta^{13}\text{C}$ values of methane ranged from 3.8 to 9.1‰ (Table 1 and supporting information Figure S5). Eight out of the remaining nine samples possessed $\delta^{13}\text{C}$ values of $\text{C}_1\text{-nC}_5$ compounds varying in a linear fashion (R^2 value > 0.9). The regression analyses yielded $\delta^{13}\text{C}$ values of hydrocarbon source from -23.4 to -19.7‰ and of pure thermogenic methane from -51.1 to -26.6‰ . The predicted $\delta^{13}\text{C}$ values of methane differed from the measured values by $< 1\text{‰}$. The analytical scheme described above was not directly applied to sample 95G925. Regression for 95G925 yielded an improbable $\delta^{13}\text{C}$ value of hydrocarbon source

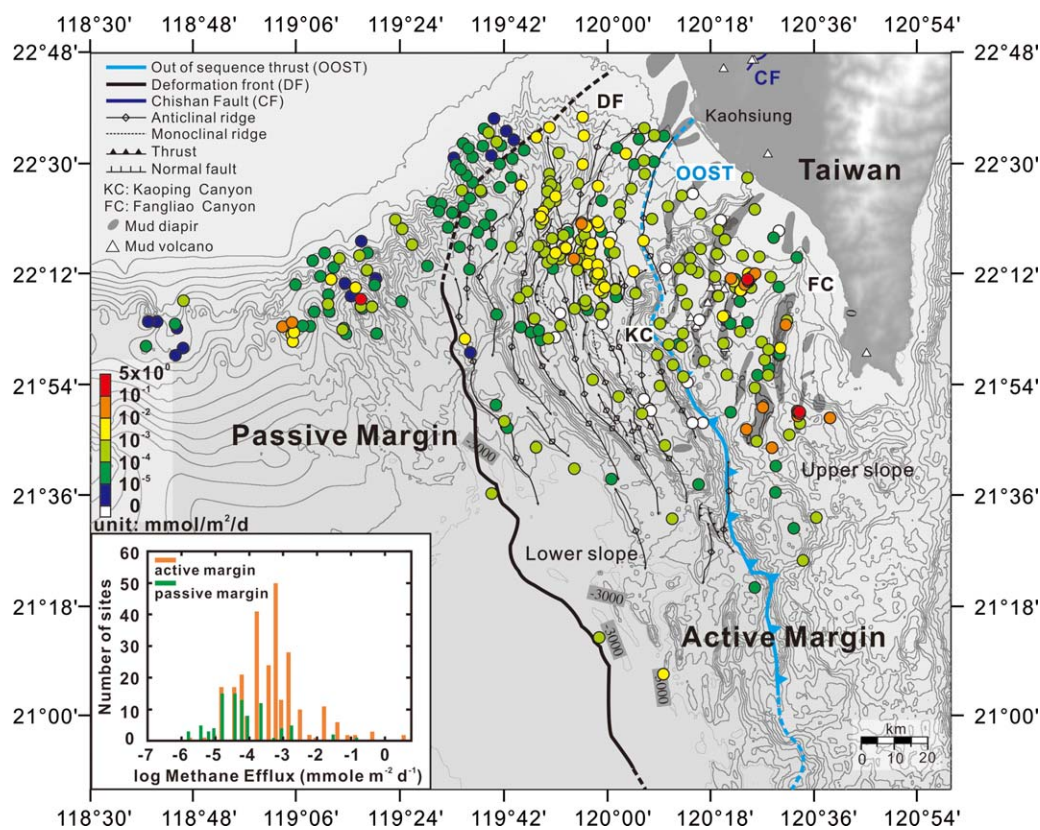


Figure 4. Methane effluxes (fluxes across the sediment-seawater interface) of the investigated area ($n = 370$). Open circles indicate negative values of fluxes. Part of data used for calculation was adopted from Chuang *et al.* [2006, 2010, 2013].

(-9.7‰) with an R^2 value of 0.92. Therefore, the data were excluded from further interpretation and discussion.

The offsets between the measured and projected $\delta^{13}\text{C-CH}_4$ values for six sets of data represent thermogenic hydrocarbons impacted by methanogenesis at various degrees. For the scenario with acetoclastic methanogenesis as microbial end-component, the contribution of microbial methane to the overall methane inventory at great depth ranged from 21 to 49% with a mean of 39%. For the scenario with hydrogenotrophic methanogenesis, the microbial contribution ranged from 10 to 24% with a mean of 17% and from 7 to 16% with a mean of 11% using isotopic fractionation factors of 40 and 60 ‰ , respectively.

Using the rock properties and geometry of the subduction wedge, thermogenic methane production rates for the investigated area (60% of onshore and offshore area) were calculated to range between 1406 and 21,979 Tg Myr^{-1} . Depending on the microbial scenarios described above, microbial processes could contribute 106–21,117 Tg Myr^{-1} methane at great depth, considering offshore and onshore areas combined.

4.4. Methane Origins

By using the Bernard plot [Bernard *et al.*, 1976], the abundance ratios of hydrocarbons against isotopic data identified the possible origin of methane (Figure 5). These data points were obtained from the deepest sample of the cores, where sulfate was depleted and methane was abundant (except for site MV12–1, a submarine mud volcano, where sulfate concentration was 10 mM and methane concentration was more than 2 mM; supporting information Table S2). The only C_1/C_{2+} ratio and the $\delta^{13}\text{C-CH}_4$ value from the passive margin (site 3264) were 935 and -90.5‰ , respectively, falling in the region of mixed microbial and thermogenic methane (Figure 5 and supporting information Table S5). Ratios of C_1 to C_{2+} for sites located at the lower slope were between 78 and 36,047, whereas the corresponding $\delta^{13}\text{C-CH}_4$ values ranged from -103.0 to -68.1‰ . Equal numbers of sites were classified into the field of purely microbial methane and a mixture of microbial and thermogenic methane. At the upper slope, C_1/C_{2+} ratios were between 9.2 and 3893 while $\delta^{13}\text{C-CH}_4$ values were in the range between -81.0 and -35.6‰ . Most $\delta^{13}\text{C-CH}_4$ values obtained from the

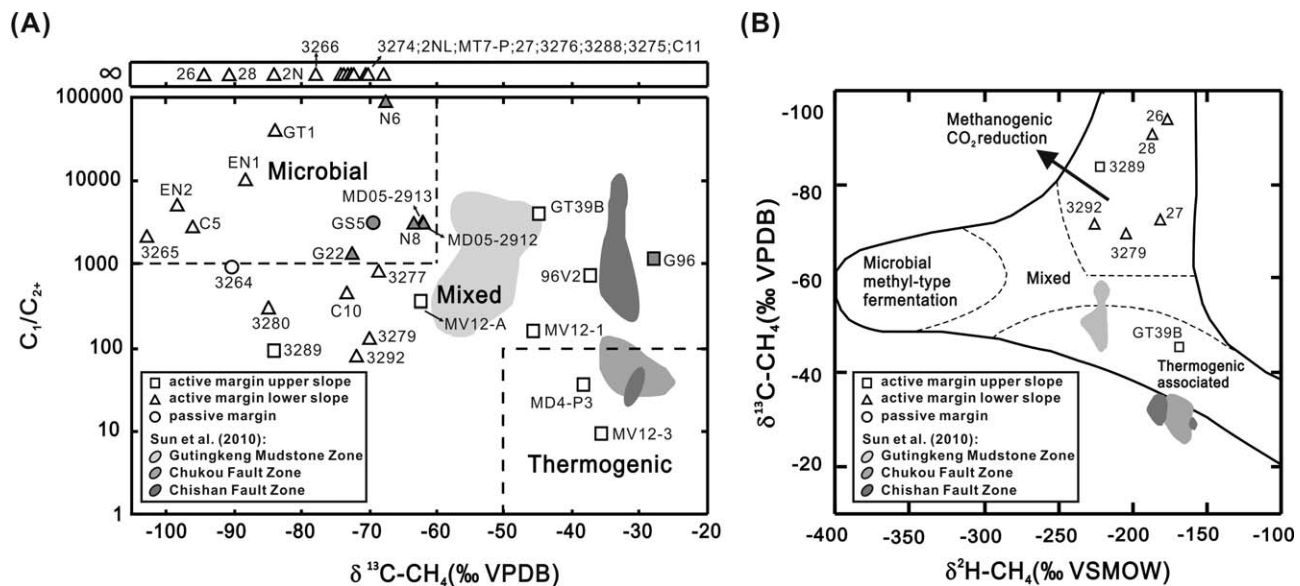


Figure 5. Plots of (a) hydrocarbon abundance ratios versus $\delta^{13}\text{C-CH}_4$ and of (b) $\delta^{13}\text{C-CH}_4$ versus $\delta^2\text{H-CH}_4$. The assignment of the region for specific gas origin is based on Bernard *et al.* [1976] and Whiticar [1999]. Data previously reported in Chuang *et al.* [2010, 2013] and terrestrial mud volcanoes in southwestern Taiwan from Sun *et al.* [2010] are shown by the gray symbols and regions, respectively. Square symbols denote data from the upper slope; triangle symbols are data from the lower slope.

upper slope were greater than -50‰ . However, their, C_1/C_{2+} ratios varied considerably. While only data from two sites (site MV12-3 and MD4-P3) fell into the field of thermogenic methane, all the other sites were in the field with mixed sources. The $\delta^2\text{H-CH}_4$ values ranged between -225 and -170‰ . These values, combined with their corresponding $\delta^{13}\text{C-CH}_4$ values, were plotted in the field of methanogenesis through CO_2 reduction for most of the samples analyzed. Only data for site GT39B fell in the field of thermogenic methane.

5. Discussion

5.1. Fluxes Across Different Interfaces and Correlations With Structural Features

The results obtained in this and previous studies [Chuang *et al.*, 2006, 2010, 2013; Ye *et al.*, 2016] indicate that except for the cold-seep sites at the Formosa Ridge, methane fluxes across the SMTZ and sediment-seawater interface (i.e., effluxes) are low in passive margins (Figures 3 and 4). In contrast, methane fluxes are elevated at the bathymetric high of the active margin, including sites from TNR, FTR, YAR, and GWR, G96 seep, and Tsanyao mud volcano (Figures 3 and 4 and supporting information Figure S4). The fluxes derived from the concentration gradient were generally comparable with those obtained by the box model calculation (i.e., within the same order of magnitude), validating the utility of diffusive fluxes to a broader area coverage.

All the ridges described above are distributed at the lower slope of the active margin, where a series of anticlines was formed by displacement of blind thrusts [Lin *et al.*, 2008, 2009, 2013]. Seismic data show that emergent thrusts exist near YAR and GWR, tilting the strata perpendicular to seafloor [Lin *et al.*, 2009]. By comparison, mud diapirism is prevalent at the upper slope. EK500 sonar-gram also reveals that a number of mud volcanoes are distributed at upper slope [Chen *et al.*, 2010, 2014; Yang *et al.*, 2014]. The intimate association between methane fluxes and structural features suggests the structurally controlled transport of methane. Migration of deeply sourced methane is facilitated by the potential fluid channels along faults and/or stratigraphic interlayers as well as by the buoyant migration associated with mud diapirism. The similar structural correlation could be also observed from the terrestrial setting where mud volcanoes in southwestern Taiwan are well aligned along NNE-SSW trending faults [Chao *et al.*, 2013]. These faults provide a fluid channel through which unconsolidated sediments with gases and fluids generated from water-rock interactions could ascend to surface environments. Although methane flux and structural feature are qualitatively correlated to a certain degree, most profiles of chloride did not indicate substantial influence of

fluid advection in shallow sediments. It is likely that rapid fluid migration only proceeded at restricted spots where structural features are directly exposed on seabed or extended to very shallow depth intervals. For the majority of investigated area, methane transport in shallow sediments is still dominated by diffusion.

5.2. Methane Origins

Our results, compiled with previous studies [Chuang *et al.*, 2010; Sun *et al.*, 2010], revealed that most methane from the passive margin and the lower slope of the active margin was microbial in origin (Figure 5). The $\delta^{13}\text{C}\text{-CH}_4$ values became greater with increasing landward distance from the passive margin, suggesting greater inputs of thermogenic gas at the active margin and onshore mud volcanoes.

Seeps and mud volcanoes at the upper slope and onshore are associated with mud diapirism and faults, respectively [Lin *et al.*, 2009, 2013]. The increasing contribution of thermogenic methane to the observed geochemical signatures suggests that the permeability of fluid channels at the upper slope and onshore is great. Therefore, thermogenic hydrocarbons formed through sediment burial at depth could transport transiently within the fluid channel with relatively limited incorporation of microbial methane formed at shallow depth. In contrast, microbial contribution to the overall methane inventory increases dramatically at the lower slope and passive margin. The transport of deeply sourced thermogenic methane could be impeded with either the overlying thick, fine-grained sediments, or low connectivity and permeability of fluid channels. As such, thermogenic methane could be trapped within the strata, thereby allowing the detection of the predominance of microbial methane formed at shallow depth. The abundance ratios and isotopic compositions, however, did not enable us to infer the possible depth range for the generation of microbial methane, even though the available deepest sample was considered. This is because any microbial methane produced could have ascended either with deeply sourced fluids over a long distance, or through diffusion within the local depth range.

The $\delta^2\text{H}$ and $\delta^{13}\text{C}$ values of methane from site GT39B located at FLR (submarine diapir), Gutingkeng Mudstone zone (terrestrial area), and Chishan Fault (terrestrial area) suggest that methane was predominantly produced by thermal maturation (Figure 5b). However, the C_1/C_{2+} ratios were higher than 1000 (Figure 5), a characteristic typical of microbial methane. Such contradictory inferences for a gas origin have also been observed in some seeps and mud volcanoes in Azerbaijan, Japan, and Italy where an inverse correlation between C_1/C_{2+} ratio and gas flux has been identified [Etioppe *et al.*, 2007, 2009]. For these examples, the abundance ratios were higher than 1000 before mud eruption (with low flux), and decreased gradually thereafter (with high flux). The temporal variations in abundance ratio or isotopic composition suggest that both fluid residence time and magnitude of isotopic fractionation might play a role in controlling the observed geochemical signatures. With a longer gas-water-mud interaction time and a smaller isotopic fractionation associated with methanogenesis, in situ microbial processes could produce methane and significantly enhance the C_1/C_{2+} ratio while maintaining low $\delta^{13}\text{C}$ values. A small isotopic fractionation has been observed for acetoclastic methanogenesis in sediments collected from the Gutingkeng Mudstone zone [Ling *et al.*, 2012], partially supporting the assertion described above.

5.3. Biofiltration Efficiency of AOM

To investigate the efficiency of microbial filtration of methane, sites with flux estimates from two interfaces (the SMTZ and sediment-seawater interface; 61 sites) were chosen (supporting information Table S1). The biofiltration efficiency (BE) of AOM was calculated as the following equation:

$$BE = \frac{\text{fluxes across SMTZ}}{\text{fluxes across SMTZ} + \text{effluxes}} \times 100\%. \quad (9)$$

Since the penetration depth of dissolved oxygen is commonly less than 1 cm [Sommer *et al.*, 2010; Boetius and Wenzhöfer, 2013], the oxygen availability for aerobic oxidation of methane (AeOM) would be greatly limited. Therefore, the methane sink catalyzed by AeOM was assumed to be negligible. Of all investigated sites (included previous studies), 51 had positive effluxes, indicating that methane escaped from sediments to overlying seawater. Although the negative fluxes could also originate from the net benthic consumption through AeOM, additional measurements of benthic fluxes for methane and oxygen would be needed to prove this assertion. These negative fluxes were excluded from further discussion. The BE values for the majority of sites were greater than 50% (supporting information Table S1), suggesting that AOM plays an important role in regulating the quantity of methane exported to seawater. The effectiveness of AOM is

also supported by the elevated DIC concentrations (supporting information Figure S2), the percentage of sulfate consumed by AOM (supporting information Table S3), and abundant anaerobic methanotrophs at the SMTZ [Lin *et al.*, 2014]. The exceptions (less effective AOM) were sites located proximal to cold seeps or with shallower SMTZ (<50 cmbsf; including cold seep G96, YAR, GWR, and area between YAR and GWR).

The BE values for offshore sediments appear to be comparable with the terrestrial counterpart. Reactive transport modeling for geochemical profiles obtained from the Shing-yang-nyu-hu MV in southwestern Taiwan indicated that sulfate-dependent AOM processes in the mud platform surrounding the bubbling pool could account for the removal of 60% of deeply sourced methane [Cheng *et al.*, 2012]. Such efficiency could have decreased to an even lower level for the mud pool, considering that fluid advection is substantial and sulfate is less abundant (14–249 μM in the pool versus ~ 4 mM in the top sediments) [Cheng *et al.*, 2012]. Overall, biological filtration of methane mediated by anaerobic methanotrophy is generally effective in sediments offshore and onshore southwestern Taiwan. However, their magnitudes in terrestrial settings might vary by a considerable magnitude, particularly at sites where fluid advection is significant.

The variation in BE value for sediments offshore southwestern Taiwan (21–100%) has also been observed in other marine methane-rich sediments (supporting information Tables S1 and S6) [Boetius and Wenzhöfer, 2013]. Sites right above cold seeps and submarine mud volcanoes are generally interpreted to be controlled by the velocity of fluid flow. Previous field observations and modeling results indicate that rapid advection would enable the advancement of oxidant-deprived fluids to very shallow depths, thereby greatly restraining the penetration of seawater sulfate and the activity of sulfate dependent anaerobic methanotrophy [Niemann *et al.*, 2006; Wallmann *et al.*, 2006b; Felden *et al.*, 2010]. As a consequence, the net flux of methane released into the seawater column would be enhanced at seeps with high advection rates [Treude *et al.*, 2003; Haese *et al.*, 2003; Wallmann *et al.*, 2006b]. Alternatively, mud volcanism and associated temperature fluctuations have been considered to inhibit benthic methane consumption [Feseker *et al.*, 2014]. In this study, the BE values for six sites proximal to cold seeps and mud diapirs were less than 50%. Although the corresponding chloride profiles do not indicate rapid fluid advection (supporting information Figure S6), the relationships between the lower BE values and seepage/mud diapirism might still suggest partial control of fluid regime on the efficiency of microbially mediated methane removal.

5.4. Fate of Methane in Taiwan Accretionary Prism: From Source to Sink

Three categories, including efflux, sink, and source of methane, were provided in Table 2 with each composed of the contributions from individual compartments or processes. Such an assessment allows us to examine the overall methane budget in a region where methane cycling and transport are highly tectonically controlled.

Considering the area sizes, the mean area-based methane effluxes were calculated to be ~ 52 Mg yr⁻¹ with the majority contributed by normal sites (46 Mg yr⁻¹; Table 2). The area-based methane effluxes from all onshore mud volcanoes in southwestern Taiwan were summed to be 130 Mg yr⁻¹ [Hong *et al.*, 2013a]. Considering the small area coverage, onshore mud volcanoes contribute disproportionately greater to methane discharge than their marine counterparts.

The primary sink considered was the methane consumptions mediated by AOM processes. To calculate the total AOM consumption, AOM rates for the hot sites and normal sites were multiplied by the area coverage to yield the area-based methane sink rates, ranging from 1.82 to 5.57 Mg yr⁻¹ and from 186 to 5970 Mg yr⁻¹ for the hot and normal sites, respectively. Although most coring operations targeted sites with high methane ebullition and higher AOM rates, the overall area-based methane sink is apparently skewed by the area size. The normal sites outcompeted the hot sites in methane removal by orders of magnitude. Methane consumptions of AOM and AeOM from terrestrial mud volcanoes were 9.48×10^{-3} and 6.17×10^{-3} Mg yr⁻¹, respectively [Cheng *et al.*, 2012]. The summed area-based methane consumption for onshore mud volcanoes were 2 orders of magnitude lower than the consumption from the offshore hot sites. Their impacts to the overall methane cycling and budget could be marginally ignored.

Major methane sources include microbial methane production in the near seafloor and deep sediments, and thermal decomposition of organic matter during subduction. For near-seafloor marine sediments, the methane production rates (CR (CO₂ reduction) + ME (methanogenesis)) estimated by the results of box model and a previous study ranged from 0.56 to 14.1×10^{-2} mmol m⁻² d⁻¹ [Chuang *et al.*, 2013]. The

Table 2. Assessment of Sources, Sinks, and Effluxes in Offshore and Onshore Southwestern Taiwan

	Flux/Rate (mmol m ⁻² d ⁻¹)	Area (km ²)	Area-Based Fluxes (Mg yr ⁻¹)	Area-Based Fluxes (Tg Myr ⁻¹)	# of Sites/ Features	References
<i>Effluxes</i>						
Efflux from onshore mud volcanoes	1 × 10 ⁻¹ to 1 × 10 ⁴	0.0089	130	130		Yang et al. [2004] and Hong et al. [2013a]
Efflux from sediment to seawater (normal sites)	1.78 × 10 ⁻⁶ to 8.92 × 10 ⁻³	11,777	0.12–613 (46 ^a)	0.12–613 (46 ^a)	225	Chuang et al. [2013] and This study
Efflux from sediment to seawater (hot sites)	1.05 × 10 ⁻² to 3.97	2.86	0.18–69.6 (6.23 ^a)	0.18–69.6 (6.23 ^a)	26	This study
Total			130–813	130–813		
<i>Sinks</i>						
Methanotrophy (onshore mud volcanoes)	0.03	0.0089	0.016	0.016	1	Cheng et al. [2012]
AOM (offshore normal sites)	0.27–8.68 × 10 ⁻²	11,777	186–5,970 (2,050 ^a)	186–5,970 (2,050 ^a)	67	Chuang et al. [2010], Lin et al. [2014], and This study
AOM (offshore hot sites)	1.04–3.18 × 10 ⁻¹	2.86	1.82–5.57 (4.01 ^a)	1.82–5.57 (4.01 ^a)	7	Chuang et al. [2010] and This study
Total			188–5,976 (2,054 ^a)	188–5,976 (2,054 ^a)		
<i>Sources</i>						
Shallow methanogenesis (onshore)	36 × 10 ⁻²	0.0089	0.01	0.01	1	Cheng et al. [2012]
Shallow methanogenesis (offshore)	0.56–14.1 × 10 ⁻²	11,780	385–9,700	385–9,700	18	Chuang et al. [2013] and This study
Deep methanogenesis (through acetoclastic methanogenesis)	0.12–23.8 × 10 ⁻²	20,260	374–21,117	374–21,117		Ling et al. [2012], Sun et al. [2008, 2010], and This study
Deep methanogenesis (through CO ₂ reduction)		20,260	106–6,941	106–6,941		Sun et al. [2008, 2010] and This study
Deep thermogenic methane	1.58–24.8 × 10 ⁻²	20,260	1,406–21,979	1,406–21,979		This study
Total			1,512–43,096	1,512–43,096		

^aMean values.

area-based rates were calculated to be 385–9700 Mg yr⁻¹ (Table 2). The methane production rate from onshore near surface sediments (0.36 mmol m⁻² d⁻¹) was larger than that in marine counterparts [Cheng et al., 2012]. However, the small area renders the contribution of near surface methanogenesis negligible (0.01 Mg yr⁻¹).

Our model calculation (equation (5)) suggests that deep microbial methanogenesis could contribute 7–49% of the overall methane production. With the estimates of 1406–21,979 Tg Myr⁻¹ of thermogenic methane produced during the sediment subduction, deep microbial methanogenesis was calculated to produce methane at an area-based rate of 106–21,117 Tg Myr⁻¹, depending on the fractionation factors used for individual pathways (Table 2).

The overall methane fluxes estimated for individual categories revealed an imbalanced budget with the deep methane production rates potentially exceeding the sum of methane consumption rates and effluxes by orders of magnitude. Since such estimates were based on specific assumptions or data coverage, several considerations are provided below to assess the accuracy and validity of individual fluxes, and to provide additional consideration that remains to be addressed in future investigation.

Of all individual fluxes, those related to offshore shallow methanogenesis and methane consumption were calculated on the basis of the box model involving reactions related to methane, organic and inorganic carbon, and sulfate transformation. For most sites investigated, the calculated AOM rates were comparable with those derived from the concentration gradient, suggesting that the reactions considered for the box model were sufficient and that the rate estimates were constrained properly. The results from the box model also suggest that shallow microbial methanogenesis was mostly offset by AOM within the SMTZ zone (within an order of magnitude; see Table 2 for the exact quantity). The calculation based on the box model described above was primarily applied to the hot sites near seeps or mud volcanoes. For the normal sites, the rates between methane production and consumption could be offset to an even greater degree, leading to a smaller methane leakage. In this way, extrapolation to the whole investigated offshore area is considered valid, even though the lack of complete data sets renders the estimate of shallow microbial methane production for all sites impossible.

The nearly equal rates between methane production and consumption for shallow offshore sediments leave the potentially imbalanced methane budget controlled by deep microbial methanogenesis and thermal

maturation. The major uncertainties associated with the estimates for deep microbial methanogenesis stemmed from the pathways and fractionation factors chosen for deep subsurface environments. A previous study has demonstrated that methanogens utilizing H_2/CO_2 , acetate, and methyl compounds are all viable in hot muddy sediments emanating from a terrestrial mud volcano [Ling *et al.*, 2012]. Molecular analyses yielded the predominance of *Methanosaeta thermophila* over the others in the archaeal community. The fractionation factors for *M. thermophila* have been experimentally determined to be less than 10‰ [Valentine *et al.*, 2004]. These fractionation factors based on pure strain are comparable with those derived from incubations amended with acetate at high temperatures for natural populations [Ling *et al.*, 2012]. The designation of a specific methanogenic pathway for our model calculation could be complicated by the small fractionation factor (<10‰) associated with hydrogenotrophic methanogens (strain 121) under extremely high pressure (>40 MPa) and temperature (>110°C) [Takai *et al.*, 2008]. With decreasing pressures and temperatures imposed, the fractionation factors would resemble those commonly observed for hydrogenotrophic methanogens. Head *et al.* [2003] and Jones *et al.* [2008] argued that methanogenesis in petroleum system proceeds with syntrophic partnerships between the fermentation of complex organic matters and hydrogenotrophic/acetoclastic methane production at $\leq 80^\circ\text{C}$ (equivalent to ~ 3 km depth or 30 MPa hydrostatic pressure, assuming a geothermal gradient of $25^\circ\text{C}/\text{km}$ and a surface temperature of 25°C). Therefore, it is likely that methanogens residing at great depths catalyze methane production with the isotopic fractionation at a magnitude across a wide range, which has been observed in a 2.5 km deep borehole offshore Japan [Inagaki *et al.*, 2015]. The current data did not allow us to attribute a specific fractionation factor or pathway to obtain a more precise estimate.

The uncertainties for estimates of thermogenic methane production through sediment subduction stem from two main factors: the sediment thickness above the subducted plate, and hydrocarbon potential (PP value). Because the South China Sea is a small marginal sea, sediment accumulation would be strongly affected by sediment discharge from the nearby Eurasian plate and islands, thereby resulting in variable sediment thicknesses in the leading Eurasian plate during the presubduction phase [Lin *et al.*, 2008]. In addition, the hydrocarbon potential could be dependent on sediment reactivity, which is intrinsically related to its source properties and transport pathways. Low TOC contents have been commonly observed for sediments offshore southwestern Taiwan (<0.7% in wt.) [Hsu *et al.*, 2014]. This range of TOC is much lower than that for sediments in other marginal basins where hydrocarbons or hydrates are abundant (e.g., >2% in the Black Sea and Ulleung Basin), and might reflect the possibility that rapid uplift, short-term soil development, strong chemical weathering and physical erosion, and multiple cycling events associated with Taiwan's tectonic configuration could have led to the reduced contents and enhanced recalcitrance of organic matter. Whether the exact hydrocarbon potential is the same as that cited in the literature remains to be determined.

The summed area-based rates of deep methane production by microbial methanogenesis and thermal maturation ranged between 1512 and 43,096 Tg Myr⁻¹. If the rates for shallow methanogenesis are assumed to offset those for AOM completely, the deep methane production rates exceed the summed effluxes of 130–813 Tg Myr⁻¹ by various degrees, regardless of which microbial scenarios are considered. The imbalance between deep methane production and efflux might be best accounted for by the presence of huge volume of gas hydrates stored in the current sediments. Using the depth and distribution of the bottom reflection simulator and temperature-pressure stability condition of methane hydrate, the potential amount of gas hydrate was estimated to be 1269 km³ or between 537 and 631 Tg in the active margin [Chung *et al.*, 2016]. Similarly, hydrocarbon gases absorbed on surface of clay minerals have been quantified to exceed the volume of free or dissolved gases in marine sediments [Ertefai *et al.*, 2010]. The capacity of clay minerals for absorbing methane is dependent on pressure imposed and in situ methanogenesis. Assuming an absorption capacity of 0.01 mmol of methane per kg of sediments [Ertefai *et al.*, 2010] and 1 km thickness of sediments, the overall quantity of methane absorbed in offshore and onshore subsurface could reach 8 Tg. An order of magnitude greater in absorption capacity and several kilometers of sediments would make the absorbed methane a significant untapped source. Nevertheless, gas hydrates and absorbed methane stored within the sediments could at least partially account for the budget imbalance described above.

Finally, the timescale represented by the measured data sets or the model calculation was unavoidably small when compared to the long-term tectonic activity. The geological background and associated organic characteristics and microbial activities were assumed to be invariant over a million year timescale. The

incorporation of field measurements into a long-term budget estimate could be biased due to the under-sampling limitation.

6. Conclusions

We have presented a systematic and comprehensive approach to quantify methane fluxes in individual compartments of the Taiwan accretionary prism. Based on the data obtained in this and previous studies, the calculated diffusive fluxes across the SMTZ and effluxes spanned over four and six orders of magnitude, respectively. Such a wide range of fluxes was controlled by the distribution of structural features, with high values generally proximal to mud diapirs, thrusts, ridges, and formation intersection. Abundance ratios combined with isotopic compositions further indicated the increasing contribution of thermogenic methane along a transect from the lower slope, to the upper slope and onshore mud volcanoes. It is likely that the permeability of fluid channeling determines the quantity of microbial methane incorporated from shallow depth. The flux calculation also indicated that biological filtration, catalyzed by AOM processes, is effective in removing >50% of methane reaching the shallow depth at most offshore and onshore investigated sites, leaving a small fraction of methane leaked into the seawater or atmosphere. The exceptions are sites located near mud diapirs or cold seeps, where high fluid flow and/or temperature fluctuation associated with mud volcanism could have inhibited microbial methane consumptions to a great degree. The calculation based on the box model not only independently validated the diffusive fluxes derived from the concentration gradient, but also indicated that the rates of methanogenesis and AOM at shallow depths were nearly balanced, a phenomenon comparable with that observed in other marginal seas. The methane fluxes at shallow depth are, however, imbalanced from those at great depth. The mass balance based on the observed isotopic compositions for field samples and incubation experiments, and the scenario configuration, projected that microbial methane could contribute 7–49% of the total methane inventory at great depth. With the wedge geometry of subduction and sediment property inferred from pre-existing data, the rates of methane production through combined microbial methanogenesis and thermal maturation was estimated to be 1512–43,096 Tg Myr⁻¹. As the effluxes were much less than the fluxes of the deep source, the methane generated at depth has to be sequestered into hydrate forms or clay minerals. The exact quantities of these two untapped components remain to be validated through other independent methods. The quantitative framework constrained by multiple methodologies highlights the possible decoupling of a deep production source from shallow methane cycles and the factors that would enable better assessments on the regional methane budget in the future.

Acknowledgments

We would like to thank the captains and crews of the R/V OR I, III, and V, and MD, and all assistants and students on board for their help in sample collections and preparation, especially Lulu Chen and Tsung-Han Yang. Cheng-Hong Chen and Li-Wen Chen gave constructive comments during the earlier phase of manuscript preparation. Methane carbon isotope analysis were conducted and assisted by Ryo Mastumoto and Akihiro Hiruta at The University of Tokyo. Central Geological Survey and Ministry of Science and Technology (MOST 105–2116-M-002–001, 105–2119-M-002–036, 106–2119-M-002–029 and 106–2116-M-002–002) provided financial supports for this study. The data used are listed in the references and supporting information Tables S1 and S2.

References

- Archer, D. E., and B. A. Buffett (2012), A two-dimensional model of the methane cycle in a sedimentary accretionary wedge, *Biogeosciences*, 9(8), 3323–3336, doi:10.5194/bg-9-3323-2012.
- Bernard, B. B., J. M. Brooks, and W. M. Sackett (1976), Natural gas seepage in the Gulf of Mexico, *Earth Planet. Sci. Lett.*, 31(1), 48–54, doi:10.1016/0012-821X(76)90095-9.
- Berner, R. A. (1980), *Early Diagenesis—A Theoretical Approach*, Princeton Univ. Press, Princeton, N. J.
- Boetius, A., and F. Wenzhöfer (2013), Seafloor oxygen consumption fuelled by methane from cold seeps, *Nat. Geosci.*, 6(9), 725–734, doi:10.1038/ngeo1926.
- Boudreau, B. P. (1997), *Diagenetic Models and Their Implementation*, vol. 505, 132 pp., Springer, Berlin.
- Boudreau, B. P., and N. L. Guinasso (1982), The influence of a modeling sublayer on accretion, dissolution, and diagenesis at the sea floor, in *The Dynamic Environment of the Ocean Floor*, edited by K. A. Fanning and F. T. Manheim, pp. 115–145, Lexington Books, Rowman & Littlefield International, Lexington, Mass.
- Chao, H. C., C. F. You, and C. H. Sun (2010), Gases in Taiwan mud volcanoes: Chemical composition, methane carbon isotopes, and gas fluxes, *Appl. Geochem.*, 25(3), 428–436, doi:10.1016/j.apgeochem.2009.12.009.
- Chao, H. C., C. F. You, H. C. Liu, and C. H. Chung (2013), The origin and migration of mud volcano fluids in Taiwan: Evidence from hydrogen, oxygen, and strontium isotopic compositions, *Geochim. Cosmochim. Acta*, 114, 29–51, doi:10.1016/j.gca.2013.03.035.
- Chen, M. P. (1981) Geotechnical properties of sediments off the coast of Hsinchu-northwest Taiwan related to sedimentary environment, *Acta Oceanogr. Taiwan*, 12, 28–53.
- Chen, S. C., S. K. Sun, C. H. Tsai, C. Y. Ku, Y. C. Yeh, and Y. Wang (2010), Gas seepage, pockmarks and mud volcanoes in the near shore of SW Taiwan, *Mar. Geophys. Res.*, 31(1–2), 133–147, doi:10.1007/s11001-010-9097-6.
- Chen, S. C., S. K. Hsu, Y. Wang, P. C. Chen, S. H. Chung, P. C. Chen, C. H. Tsai, C. S. Liu, H. S. Lin, and Y. W. Lee (2014), Distribution and characters of the mud diapirs and mud volcanoes off southwest Taiwan, *J. Asian Earth Sci.*, 92, 201–214, doi:10.1016/j.jseas.2013.10.009.
- Cheng, T. W., Y. H. Chang, S. L. Tang, C. H. Tseng, P. W. Chiang, K. T. Chang, C. H. Sun, Y. G. Chen, H. C. Kuo, and C. H. Wang (2012), Metabolic stratification driven by surface and subsurface interactions in a terrestrial mud volcano, *ISME J.*, 6(12), 2280–2290, doi:10.1038/ismej.2012.61.
- Chi, W. C., and D. L. Reed (2008), Evolution of shallow, crustal thermal structure from subduction to collision: An example from Taiwan, *Geol. Soc. Am. Bull.*, 120(5–6), 679–690, doi:10.1130/B26210.1.

- Chi, W. C., D. L. Reed, G. Moore, T. Nguyen, C. S. Liu, and N. Lundberg (2003), Tectonic wedging along the rear of the offshore Taiwan accretionary prism, *Tectonophysics*, 374(3), 199–217, doi:10.1016/j.tecto.2003.08.004.
- Chiang, C. S., H. S. Yu, and Y. W. Chou (2004), Characteristics of the wedge-top depozone of the southern Taiwan foreland basin system, *Basin Res.*, 16(1), 65–78, doi:10.1111/j.1365-2117.2004.00222.x.
- Chuang, P. C., T. F. Yang, S. Lin, H. F. Lee, T. F. Lan, W. L. Hong, C. S. Liu, J. C. Chen, and Y. Wang (2006), Extremely high methane concentration in bottom water and cored sediments from offshore southwestern Taiwan, *Terr. Atmos. Oceanic Sci.*, 17(4), 903–920.
- Chuang, P. C., T. F. Yang, W. L. Hong, S. Lin, C. H. Sun, A. T. S. Lin, J. C. Chen, Y. Wang, and S. H. Chung (2010), Estimation of methane flux offshore SW Taiwan and the influence of tectonics on gas hydrate accumulation, *Geofluids*, 10, 497–510, doi:10.1111/j.1468-8123.2010.00313.x.
- Chuang, P. C., et al. (2013), Relating sulfate and methane dynamics to geology: The accretionary prism offshore SW Taiwan, *Geochem. Geophys. Geosyst.*, 14, 2523–2545, doi:10.1002/ggge.20168.
- Chung, H. M., J. R. Gormly, and R. M. Squires (1988), Origin of gaseous hydrocarbons in subsurface environments: Theoretical considerations of carbon isotope distribution, *Chem. Geol.*, 71, 97–104, doi:10.1016/0009-2541(88)90108-8.
- Chung, S. H., A. T. Lin, C. C. Lin, C. S. Liu, S. C. Chen, Y. Wang, C. Y. Wei, and P. C. Chen (2016), Geological investigation of gas hydrate resource potential in the offshore areas of south-southwest Taiwan [in Chinese with English abstract], *Cent. Geol. Surv. Spec. Publ.*, 30, 1–42.
- Dadson, S. J., N. Hovius, H. Chen, W. B. Dade, M.-L. Hsieh, S. D. Willett, J.-C. Hu, M.-J. Horng, M.-C. Chen, and C. P. Stark (2003), Links between erosion, runoff variability and seismicity in the Taiwan orogen, *Nature*, 426, 648–651, doi:10.1038/nature02150.
- Dale, A. W., P. Regnier, N. J. Knab, B. B. Jørgensen, and P. Van Cappellen (2008a), Anaerobic oxidation of methane (AOM) in marine sediments from the Skagerrak (Denmark): II. Reaction-transport modeling, *Geochim. Cosmochim. Acta*, 72(12), 2880–2894, doi:10.1016/j.gca.2007.11.039.
- Dale, A. W., P. Van Cappellen, D. R. Aguilera, and P. Regnier (2008b), Methane efflux from marine sediments in passive and active margins: Estimations from modeling bioenergetic reaction-transport simulations, *Earth Planet. Sci. Lett.*, 265(3–4), 329–344, doi:10.1016/j.epsl.2007.09.026.
- Dale, A. W., S. Sommer, M. Haeckel, K. Wallmann, P. Linke, G. Wegener, and O. Pfannkuche (2010), Pathways and regulation of carbon, sulfur and energy transfer in marine sediments overlying methane gas hydrates on the Opouawe Bank (New Zealand), *Geochim. Cosmochim. Acta*, 74(20), 5763–5784, doi:10.1016/j.gca.2010.06.038.
- Dickens, G. R., J. R. Oneil, D. K. Rea, and R. M. Owen (1995), Dissociation of oceanic methane hydrate as a cause of the carbon-isotope excursion at the end of the Paleocene, *Paleoceanography*, 10(6), 965–971, doi:10.1029/95PA02087.
- Ertefai, T. F., V. B. Heuer, X. Prieto-Mollar, C. Vogt, S. P. Sylva, J. Seewald, and K. U. Hinrichs (2010), The biogeochemistry of sorbed methane in marine sediments, *Geochim. Cosmochim. Acta*, 74(21), 6033–6048, doi:10.1016/j.gca.2010.08.006.
- Etiopie, G., G. Martinelli, A. Caracausi, and F. Italiano (2007), Methane seeps and mud volcanoes in Italy: Gas origin, fractionation and emission to the atmosphere, *Geophys. Res. Lett.*, 34, L14303, doi:10.1029/2007GL030341.
- Etiopie, G., A. Feyzullayev, and C. L. Baciú (2009), Terrestrial methane seeps and mud volcanoes: A global perspective of gas origin, *Mar. Pet. Geol.*, 26(3), 333–344, doi:10.1016/j.marpetgeo.2008.03.001.
- Felden, J., F. Wenzhöfer, T. Feseker, and A. Boetius (2010), Transport and consumption of oxygen and methane in different habitats of the Håkon Mosby Mud Volcano (HMMV), *Limnol. Oceanogr.*, 55(6), 2366–2380, doi:10.4319/lo.2010.55.6.2366.
- Feseker, T., A. Boetius, F. Wenzhöfer, J. Blandin, K. Olu, D. R. Yoerger, R. Camilli, C. R. German, and D. De Beer (2014), Eruption of a deep-sea mud volcano triggers rapid sediment movement, *Nat. Commun.*, 5, 5385, doi:10.1038/ncomms5385.
- Forster, P., et al. (2007), Changes in atmospheric constituents and in radiative forcing, in *Climate Change 2007. The Physical Science Basis*. Haese, R. R., C. Meile, P. Van Cappellen, and G. J. De Lange (2003), Carbon geochemistry of cold seeps: Methane fluxes and transformation in sediments from Kazan mud volcano, eastern Mediterranean Sea, *Earth Planet. Sci. Lett.*, 212(3–4), 361–375, Cambridge University Press, Cambridge, U. K., doi:10.1016/S0012-821X(03)00226-7.
- Head, I. M., D. M. Jones, and S. R. Larter (2003), Biological activity in the deep subsurface and the origin of heavy oil, *Nature*, 426(6964), 344–352, doi:10.1038/nature02134.
- Hong, W. L., G. Etiopie, T. F. Yang, and P. Y. Chang (2013a), Methane flux from miniseepage in mud volcanoes of SW Taiwan: Comparison with the data from Italy, Romania, and Azerbaijan, *J. Asian Earth Sci.*, 65, 3–12, doi:10.1016/j.jseae.2012.02.005.
- Hong, W. L., M. E. Torres, J. H. Kim, J. Choi, and J. J. Bahk (2013b), Carbon cycling within the sulfate-methane-transition-zone in marine sediments from the Ulleung Basin, *Biogeochemistry*, 115(1–3), 129–148, doi:10.1007/s10533-012-9824-y.
- Hong, W. L., S. Sauer, G. Panieri, W. G. Ambrose, R. H. James, A. Plaza-Faverola, and A. Schneider (2016), Removal of methane through hydrological, microbial, and geochemical processes in the shallow sediments of pockmarks along eastern Vestnesa Ridge (Svalbard), *Limnol. Oceanogr.*, 61, S324–S343, doi:10.1002/lno.10299.
- Hong, W. L., M. E. Torres, J. Carroll, A. Cremiere, G. Panieri, H. Yao, and P. Serov (2017), Seepage from an Arctic shallow marine gas hydrate reservoir is insensitive to momentary ocean warming, *Nat. Commun.*, 8, 15745, doi:10.1038/ncomms15745.
- Hu, C. Y., et al. (2017), Biogeochemical cycles at the sulfate-methane transition zone (SMTZ) and geochemical characteristics of the pore fluids offshore southwestern Taiwan, *J. of Asian Earth Sci.*, doi:10.1016/j.jseae.2017.07.002.
- Huang, C. Y., P. B. Yuan, and S. J. Tsao (2006), Temporal and spatial records of active arc continent collision in Taiwan: A synthesis, *Bull. Geol. Soc. Am.*, 118, 274–288, doi:10.1130/B25527.1.
- Hunt, J. M. (1996), The origin of natural gas, in *Petroleum Geochemistry and Geology*, pp. 186–232, W. H. Freeman, New York.
- Hsu, F. H., C. C. Su, C. H. Wang, S. Lin, J. Liu, and C. A. Huh (2014), Accumulation of terrestrial organic carbon on an active continental margin offshore southwestern Taiwan: Source-to-sink pathways of river-borne organic particles, *J. Asian Earth Sci.*, 91, 163–173, doi:10.1016/j.jseae.2014.05.006.
- Inagaki, F., et al. (2015), Exploring deep microbial life in coal-bearing sediment down to ~2.5 km below the ocean floor, *Science*, 349(6246), 420–424, doi:10.1126/science.aaa6882.
- Jähne, B., G. Heinz, and W. Dietrich (1987), Measurement of the diffusion coefficients of sparingly soluble gases in water, *J. Geophys. Res.*, 92(C10), 10,767–10,776, doi:10.1029/JC092iC10p10767.
- James, A. T., and B. J. Burns (1984), Microbial alteration of subsurface natural gas accumulations, *AAPG Bull.*, 68(8), 957–960.
- Jones, D. M., et al. (2008), Crude-oil biodegradation via methanogenesis in subsurface petroleum reservoirs, *Nature*, 451(7175), 176–180, doi:10.1038/nature06484.
- Jørgensen, B. B., and D. J. Des Marais (1990), The diffusive boundary layer of sediments: Oxygen microgradients over a microbial mat, *Limnol. Oceanogr.*, 35(6), 1343–1355.
- Judd, A. G., and M. Hovland (2007), *Seabed Fluid Flow: The Impact of Geology, Biology and the Marine Environment*, Cambridge Univ. Press, Cambridge, U. K.

- Kastner, M., H. Elderfield, and J. B. Martin (1991), Fluids in convergent margins: What do we know about their composition, origin, role in diagenesis and importance for oceanic chemical fluxes?, *Philos. Trans. A*, 335(1638), 243–259, doi:10.1098/rsta.1991.0045.
- Katz, B. J., A. Narimanov, and R. Huseinzadeh (2002), Significance of microbial processes in gases of the South Caspian basin, *Mar. Pet. Geol.*, 19(6), 783–796, doi:10.1016/S0264-8172(02)00086-7.
- Kennett, J. P., and B. N. Fackler-Adams (2000), Relationship of clathrate instability to sediment deformation in the upper Neogene of California, *Geology*, 28(3), 215–218, doi:10.1130/0091-7613(2000)28<215:ROCITS>2.0.CO;2.
- Kim, J. H., M. H. Park, U. Tsunogai, T. J. Cheong, B. J. Ryu, Y. J. Lee, H. C. Han, J. H. Oh, and H. W. Chang (2007), Geochemical characterization of the organic matter, pore water constituents and shallow methane gas in the eastern part of the Ulleung Basin, East Sea (Japan Sea), *Isl. Arc*, 16(1), 93–104, doi:10.1111/j.1440-1738.2007.00560.x.
- Lelieveld, J. O. S., P. J. Crutzen, and F. J. Dentener (1998), Changing concentration, lifetime and climate forcing of atmospheric methane, *Tellus, Ser. B*, 50(2), 128–150, doi:10.1034/j.1600-0889.1998.t01-1-00002.x.
- Liao, W. Z., A. T. Lin, C. S. Liu, J. N. Oung, and Y. Wang (2016), A study on tectonic and sedimentary development in the rifted northern continental margin of the South China Sea near Taiwan, *Interpretation*, 4(3), SP47–SP65, doi:10.1190/INT-2015-0209.1.
- Lin, A. T., C. S. Liu, C. C. Lin, P. Schnurle, G. Y. Chen, W. Z. Liao, L. S. Teng, H. J. Chuang, and M. S. Wu (2008), Tectonic features associated with the overriding of an accretionary wedge on top of a rifted continental margin: An example from Taiwan, *Mar. Geol.*, 255(3), 186–203, doi:10.1016/j.margeo.2008.10.002.
- Lin, C. C., A. T. Lin, C. S. Liu, G. Y. Chen, W. Z. Liao, and P. Schnurle (2009), Geological controls on BSR occurrences in the incipient arc-continent collision zone off southwest Taiwan, *Mar. Pet. Geol.*, 26(7), 1118–1131, doi:10.1016/j.marpetgeo.2008.11.002.
- Lin, C. C., A. T. Lin, C. S. Liu, C. S. Horng, G. Y. Chen, and Y. Wang (2013), Canyon-infilling and gas hydrate occurrences in the frontal fold of the offshore accretionary wedge off southern Taiwan, *Mar. Geophys. Res.*, 35(1), 21–35, doi:10.1007/s11001-013-9203-7.
- Lin, L. H., L. W. Wu, T. W. Cheng, W. X. Tu, J. R. Lin, T. F. Yang, P. C. Chen, Y. Wang, and P. L. Wang (2014), Distributions and assemblages of microbial communities along a sediment core retrieved from a potential hydrate-bearing region offshore southwestern Taiwan, *J. Asian Earth Sci.*, 92, 276–292, doi:10.1016/j.jseae.2014.02.014.
- Ling, Y. C., Y. J. Chen, C. H. Sun, T. W. Cheng, P. L. Wang, and L. H. Lin (2012), Potential of microbial methane formation in a high-temperature hydrocarbon seep, *Appl. Geochem.*, 27(8), 1666–1678, doi:10.1016/j.apgeochem.2012.04.002.
- Linke, P., K. Wallmann, E. Suess, C. Hensen, and G. Rehder (2005), In situ benthic fluxes from an intermittently active mud volcano at the Costa Rica convergent margin, *Earth Planet. Sci. Lett.*, 235(1), 79–95, doi:10.1016/j.epsl.2005.03.009.
- Luff, R., and K. Wallmann (2003), Fluid flow, methane fluxes, carbonate precipitation and biogeochemical turnover in gas hydrate-bearing sediments at Hydrate Ridge, Cascadia Margin: Numerical modeling and mass balances, *Geochim. Cosmochim. Acta*, 67(18), 3403–3421, doi:10.1016/S0016-7037(03)00127-3.
- Lundberg, N., D. L. Reed, C. S. Liu, and J. Lieske (1997), Forearc-basin closure and arc accretion in the submarine suture zone south of Taiwan, *Tectonophysics*, 274(1), 5–23, doi:10.1016/S0040-1951(96)00295-8.
- Milkov, A. V. (2004), Global estimates of hydrate-bound gas in marine sediments: How much is really out there?, *Earth Sci. Rev.*, 66(3), 183–197, doi:10.1016/j.earscirev.2003.11.002.
- Milkov, A. V., and L. Dzou (2007), Geochemical evidence of secondary microbial methane from very slight biodegradation of undersaturated oils in a deep hot reservoir, *Geology*, 35, 455–458, doi:10.1130/G23557A.1.
- Milkov, A. V., G. E. Claypool, Y. J. Lee, and R. Sassen (2005), Gas hydrate systems at Hydrate Ridge offshore Oregon inferred from molecular and isotopic properties of hydrate-bound and void gases, *Geochim. Cosmochim. Acta*, 69(4), 1007–1026, doi:10.1016/j.gca.2004.08.021.
- Niemann, H., et al. (2006), Novel microbial communities of the Haakon Mosby mud volcano and their role as a methane sink, *Nature*, 443(7113), 854–858, doi:10.1038/nature05227.
- Pohlman, J. W., J. E. Bauer, E. A. Canuel, K. S. Grabowski, D. L. Knies, C. S. Mitchell, M. J. Whiticar, and R. B. Coffin (2009), Methane sources in gas hydrate-bearing cold seeps: Evidence from radiocarbon and stable isotopes, *Mar. Chem.*, 115(3–4), 102–109, doi:10.1016/j.marchem.2009.07.001.
- Reeburgh, W. S. (2007), Oceanic methane biogeochemistry, *Chem. Rev.*, 107(2), 486–513, doi:10.1021/cr050362v.
- Reed, D., N. Lundberg, C. S. Liu, and B. Y. Kuo (1992), Structural relations along the margins of the offshore Taiwan accretionary wedge: Implications for accretion and crustal kinematics, *Acta Geol. Taiwan*, 30, 105–122.
- Schmoker, J. W. (1994), Volumetric calculation of hydrocarbons generated, in *The Petroleum System—From Source to Trap*, pp. 323–326, Am. Assoc. of Pet. Geol., American Association of Petroleum Geologists (AAPG Bookstore), Tulsa, Okla.
- Sinclair, A. J. (1974), Selection of threshold values in geochemical data using probability graphs, *J. Geochem. Explor.*, 3, 129–149, doi:10.1016/0375-6742(74)90030-2.
- Sommer, S., O. Pfannkuche, P. Linke, R. Luff, J. Greinert, M. Drews, S. Gubsch, M. Pieper, M. Poser, and T. Viergutz (2006), Efficiency of the benthic filter: Biological control of the emission of dissolved methane from sediments containing shallow gas hydrates at Hydrate Ridge, *Global Biogeochem. Cycles*, 20, GB2019, doi:10.1029/2004GB002389.
- Sommer, S., P. Linke, O. Pfannkuche, H. Niemann, and T. Treude (2010), Benthic respiration in a seep habitat dominated by dense beds of ampharetid polychaetes at the Hikurangi Margin (New Zealand), *Mar. Geol.*, 272(1), 223–232, doi:10.1016/j.margeo.2009.06.003.
- Sun, C. H., C. L. Kuo, S. C. Chang, and S. H. Wu (2008), Hydrocarbon seepages of Kaohsiung foothills, southwestern Taiwan, *Pet. Geol. Taiwan*, 38, 117–133.
- Sun, C. H., S. C. Chang, C. L. Kuo, J. C. Wu, P. H. Shao, and J. N. Oung (2010), Origins of Taiwan's mud volcanoes: Evidence from geochemistry, *J. Asian Earth Sci.*, 37(2), 105–116, doi:10.1016/j.jseae.2009.02.007.
- Suppe, J. (1981), Mechanics of mountain building and metamorphism in Taiwan, *Mem. Geol. Soc. China*, 4(6), 67–89.
- Takai, K., K. Nakamura, T. Toki, U. Tsunogai, M. Miyazaki, J. Miyazaki, H. Hirayama, S. Nakagawa, T. Nunoura, and K. Horikoshi (2008), Cell proliferation at 122°C and isotopically heavy CH₄ production by a hyperthermophilic methanogen under high-pressure cultivation, *Proc. Natl. Acad. Sci. U. S. A.*, 105, 10,949–11,954, doi:10.1073/pnas.0712334105.
- Teng, L. S. (1996), Extensional collapse of the northern Taiwan mountain belt, *Geology*, 24(10), 949–952, doi:10.1130/0091-7613.
- Treude, T., A. Boetius, K. Knittel, K. Wallmann, and B. B. Jørgensen (2003), Anaerobic oxidation of methane above gas hydrates at Hydrate Ridge, NE Pacific Ocean, *Mar. Ecol. Prog. Ser.*, 264, 1–14.
- Ussler, W., and C. K. Paull (2008), Rates of anaerobic oxidation of methane and authigenic carbonate mineralization in methane-rich deep-sea sediments inferred from models and geochemical profiles, *Earth Planet. Sci. Lett.*, 266(3–4), 271–287, doi:10.1016/j.epsl.2007.10.056.
- Valentine, D. L., A. Chidthaisong, A. Rice, W. S. Reeburgh, and S. C. Tyler (2004), Carbon and hydrogen isotope fractionation by moderately thermophilic methanogens, *Geochim. Cosmochim. Acta*, 68(7), 1571–1590, doi:10.1016/j.gca.2003.10.012.

- von Huene, R., and D. W. Scholl (1991), Observations at convergent margins concerning sediment subduction, subduction erosion, and the growth of continental crust, *Rev. Geophys.*, *29*(3), 279–316, doi:10.1029/91RG00969.
- Wallmann, K., G. Aloisi, M. Haeckel, A. Obzhirov, G. Pavlova, and P. Tishchenko (2006a), Kinetics of organic matter degradation, microbial methane generation, and gas hydrate formation in anoxic marine sediments, *Geochim. Cosmochim. Acta*, *70*(15), 3905–3927, doi:10.1016/j.gca.2006.06.003.
- Wallmann, K., M. Drews, G. Aloisi, and G. Bohrmann (2006b), Methane discharge into the Black Sea and the global ocean via fluid flow through submarine mud volcanoes, *Earth Planet. Sci. Lett.*, *248*(1), 545–560, doi:10.1016/j.epsl.2006.06.026.
- Wallmann, K., E. Pinero, E. Burwicz, M. Haeckel, C. Hensen, A. Dale, and L. Ruppke (2012), The global inventory of methane hydrate in marine sediments: A theoretical approach, *Energies*, *5*(7), 2449–2498, doi:10.3390/en5072449.
- Wang, P., et al. (2000), *Proceedings Ocean Drilling Program Initial Reports*, vol. 184, Texas A&M Univ., College Station, Tex.
- Wang, P. L., Y. P. Chiu, T. W. Cheng, Y. H. Chang, W. X. Tu, and L. H. Lin (2014), Spatial variations of community structures and methane cycling across a transect of Lei-Gong-Hou mud volcanoes in eastern Taiwan, *Front. Microbiol.*, *5*, 121, doi:10.3389/fmicb.2014.00121.
- Whiticar, M. J. (1999), Carbon and hydrogen isotope systematics of bacterial formation and oxidation of methane, *Chem. Geol.*, *161*(1–3), 291–314, doi:10.1016/S0009-2541(99)00092-3.
- Yang, T. F., G. H. Yeh, C. C. Fu, C. C. Wang, T. F. Lan, H. F. Lee, G. H. Chen, W. Vivek, and Q. C. Sung (2004), Composition and exhalation flux of gases from mud volcanoes in Taiwan, *Environ. Geol.*, *46*(8), 1003–1011, doi:10.1007/s00254-004-1086-0.
- Yang, T. H., T. F. Yang, N. C. Chen, S. Lin, P. L. Wang, and S. K. Hsu (2014), Temporal variations of methane flux from submarine mud volcanoes off southwest Taiwan, Abstract in the 12th International Conference of Gas in Marine Sediments, Ministry of Science and Technology, Taipei, Taiwan.
- Ye, H., T. Yang, G. Zhu, S. Jiang, and L. Wu (2016), Pore water geochemistry in shallow sediments from the northeastern continental slope of the South China Sea, *Mar. Pet. Geol.*, *75*, 68–82, doi:10.1016/j.marpetgeo.2016.03.010.
- Yeh, Y. C., and S. K. Hsu (2004), Crustal structures of the northernmost South China Sea: Seismic reflection and gravity modeling, *Mar. Geophys. Res.*, *25*(1–2), 45–61, doi:10.1007/s11001-005-0732-6.
- Yoshinaga, M. Y., T. Holler, T. Goldhammer, G. Wegener, J. W. Pohlman, B. Brunner, M. M. M. Kuypers, K. U. Hinrichs, and M. Elvert (2014), Carbon isotope equilibration during sulphate-limited anaerobic oxidation of methane, *Nat. Geosci.*, *7*(3), 190–194, doi:10.1038/ngeo2069.